iScience

CellPress
OPEN ACCESS

Review

3D-printed microneedles in biomedical applications

Sajjad Rahmani Dabbagh,[1,2,9] Misagh Rezapour Sarabi,[1,9] Reza Rahbarghazi,[3,4] Emel Sokullu,[5] Ali K. Yetisen,[6] and Savas Tasoglu[1,2,7,8,*]

SUMMARY

Conventional needle technologies can be advanced with emerging nano- and micro-fabrication methods to fabricate microneedles. Nano-/micro-fabricated microneedles seek to mitigate penetration pain and tissue damage, as well as providing accurately controlled robust channels for administrating bioagents and collecting body fluids. Here, design and 3D printing strategies of microneedles are discussed with emerging applications in biomedical devices and healthcare technologies. 3D printing offers customization, cost-efficiency, a rapid turnaround time between design iterations, and enhanced accessibility. Increasing the printing resolution, the accuracy of the features, and the accessibility of low-cost raw printing materials have empowered 3D printing to be utilized for the fabrication of microneedle platforms. The development of 3D-printed microneedles has enabled the evolution of pain-free controlled release drug delivery systems, devices for extracting fluids from the cutaneous tissue, biosignal acquisition, and point-of-care diagnostic devices in personalized medicine.

INTRODUCTION

Microneedles (MNs) are devices composed of various materials such as polymers, ceramics, and metals, designed with the purpose of epidermal and intradermal delivery of vaccines, bioactive molecules, or recreational agents and also collecting substances and bio-signals from the body (Chang et al., 2017; Ren et al., 2017) while decreasing insertion pain and minimizing tissue damage. The first report of the term "microneedle" dates back to 1921 (Chambers, 1921), as a means of micro-dissection of echinoderm eggs. The concept of MNs for drug delivery was reported in 1971, including both solid and hollow MNs (Gerstel and Place, 1976). Subsequently, the first drug-coated MN was patented in 1975 (Pistor, 1975). In 1998, the first use of MN for *in vivo* studies was reported (Henry et al., 1998), followed by genetic material delivery (2001) (Bevers, 2001), vaccine delivery by MNs (2002) (Mikszta et al., 2002), MN-assisted delivery of nano-particles (2003) (McAllister et al., 2003), dissolvable MNs (2005) (Miyano et al., 2005), hollow MNs for sample extraction (2005) (Mukerjee et al., 2004; Wang et al., 2005), cosmetic application of MNs (2005) (Fernandes, 2005), and MNs in diagnostic applications (2005) (Bhatnagar et al., 2017).

MNs are an emerging subset of devices to exploit the physiology of skin tissue, the human body's largest organ with an area around 1.5–2.0 m^2 on an adult (Gallo, 2017). Figure 1 depicts the inner structure and different layers of human skin. In terms of anatomical and histological structure, cutaneous tissue is a waterproof external barrier to prevent the entrance of different biomolecules into the body, whereas this natural structure is helpful for *in situ* and systemic delivery of therapeutic agents (Yang et al., 2019). Cutaneous tissue consists of three layers: epidermis, dermis, and hypodermis (Figure 1B). The epidermis is the outermost of the three layers composed of tightly packed epithelial cells with a continuous sheet. Histologically, the epidermis is made up of two distinct layers: stratum corneum and viable epidermis. Stratum corneum, which consists of dead keratinized epithelial cells, has a thickness of 10–40 μm. The hydrophobic nature of stratum corneum prohibits the entry of biomolecules and exogenous components. The epidermis layer has multilayer epithelial cell sheets of 100–200 μm thickness. The dermis is a dense connective tissue that harbors blood vessels, nerves, hair follicles, and sebaceous and sweat glands (Russell et al., 2008). The hypodermis (subcutaneous layer) lies beneath the dermis and is composed of loosely fatty and connective tissues (Ni et al., 2020). Therefore, MNs with proper design and size can pierce the outermost layer of skin and reach underneath layers to either deliver drugs and reagents or to acquire signals or samples.

[1]Department of Mechanical Engineering, Koç University, Sariyer, Istanbul 34450, Turkey

[2]Koç University Arçelik Research Center for Creative Industries (KUAR), Koç University, Sariyer, Istanbul 34450, Turkey

[3]Stem Cell Research Center, Tabriz University of Medical Sciences, Tabriz 5165665811, Iran

[4]Department of Applied Cell Sciences, Faculty of Advanced Medical Sciences, Tabriz University of Medical Sciences, Tabriz 5166653431, Iran

[5]Koc University School of Medicine, Koç University, Sariyer, Istanbul 34450, Turkey

[6]Department of Chemical Engineering, Imperial College London, London SW7 2AZ, UK

[7]Koc University Research Center for Translational Medicine, Koç University, Sariyer, Istanbul 34450, Turkey

[8]Boğaziçi Institute of Biomedical Engineering, Boğaziçi University, Çengelköy, Istanbul 34684, Turkey

[9]These authors contributed equally

*Correspondence: stasoglu@ku.edu.tr

https://doi.org/10.1016/j.isci.2020.102012

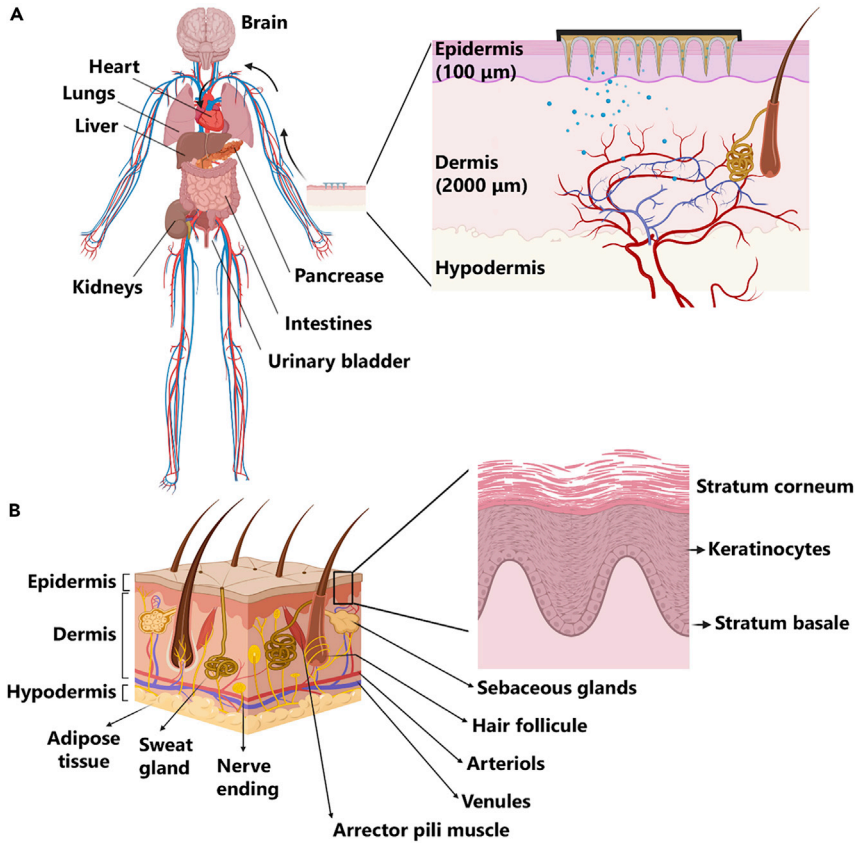

Figure 1. The main purpose of the microneedles (MNs) patch application is to deliver the active biomolecules to the close or remote sites inside the body

(A) A cutaneous tissue consists of three layers: epidermis, dermis, and hypodermis.

(B) The outermost layer, the epidermis, is a keratinized stratified squamous epithelium with closely packed epithelial cells. The dermis layer lies beneath the epidermis and is composed of connective tissue with vessels and nerves ending. The innermost layer of the skin is so-called hypodermis, which is characterized by the loose connective tissue and the existence of adipocytes.

Fabrication strategies for MNs include micromilling (wet and/or dry cutting) (García-López et al., 2018); wet and dry etching (Li et al., 2019); photolithography, which can also be combined with thermal- and photo-polymerization (Kathuria et al., 2020; Knowlton et al., 2017b); molding-based techniques (Chen et al., 2019a); cleanroom-free molding (Nejad et al., 2018); injection molding (Li et al., 2017); laser patterning (Donnelly et al., 2011); drawing lithography (Chen et al., 2018); and photolithography with an elastocapillarity-driven self-assembly mechanism (Lim et al., 2018). Many of these conventional fabrication methods have some limitations in cost-efficiency, requiring manual steps and being labor-intensive. Hence, accessible, and cost-efficient technologies are needed for the production of MNs.

3D printing is an additive manufacturing process that creates structures, prototypes, and architectures in a layer-by-layer fashion via the translation of a 3D computer-aided design (CAD) model input to a physical object. The process of 3D printing can be categorized as vat polymerization, material extrusion, material as well as binder jetting, and powder bed fusion (Ligon et al., 2017). Each 3D printing method has a unique set of tradeoffs in resolution, cost-efficiency, biocompatibility, and output volume, enabling the use of 3D printing in a wide range of applications (Bakhshinejad and D'souza, 2015; Park et al., 2015). The ability to use biomaterials in 3D printing processes (Chia and Wu, 2015), along with microscale and nanoscale 3D printing (You et al., 2018), can enable the fabrication of a wide range of laboratory instruments for clinical and point-of-care applications (Aimar et al., 2019; Amin et al., 2016b; Douroumis, 2019; Knowlton et al., 2015c; Yenilmez et al., 2016a), including organ-on-a-chip devices (Jain et al., 2020; Knowlton and Tasoglu, 2016; Knowlton et al., 2016b, 2016c), tissue engineering (Knowlton et al., 2018; Sears et al., 2016; Zhang

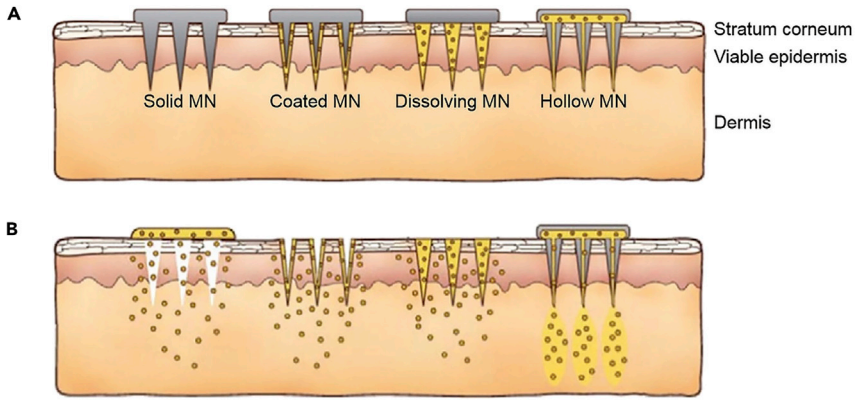

Figure 2. An illustration of the different types of microneedles (MNs) and delivery means

(A) The most common types of MNs are solid, coated, dissolving, and hollow.

(B) MNs pass drugs through the outermost layers of skin to deliver desired cargo to the dermis layer, with different approaches (Kim et al., 2012). Adapted with permission from (Kim et al., 2012). Copyright 2013, Elsevier.

et al., 2019), wound healing (Joseph et al., 2019; Tabriz et al., 2020), fertility and embryology research (Kanakasabapathy et al., 2019; Knowlton et al., 2015d; Potluri et al., 2018), cancer research (Knowlton et al., 2015a, 2016a), stem cell research (Javaid and Haleem, 2020; Tasoglu and Demirci, 2013), and circulating tumor cell isolation (Chen et al., 2020).

3D printing can address the limitations in the fabrication of MNs and microneedle arrays (MNAs). Here, 3D printing methods are introduced from the perspective of materials and technology. Emerging applications of 3D-printed MNs in biomedical engineering and healthcare systems are reviewed. These applications include drugs or bioagents delivery, sample extraction from the human body (Economidou et al., 2019; Luzuriaga et al., 2018; Miller et al., 2018), single-cell analysis (Kavaldzhiev et al., 2017), and biological signal acquisition (Ren et al., 2017).

FABRICATION OF MNS

Design structures and materials

MNs are classified into coated, solid, hollow, hydrogel-based, porous, and swellable formats, which can feature complex shapes such as honeybee inspired, angled, and arrow-head MNs (Figure 2) (Camović et al., 2019; Krieger et al., 2019). Enabling high-throughput fabrication of MNs requires a high uniformity in their structures (Nejad et al., 2018). Several geometrical factors such as MNs' height, width, aspect ratio, and tip thickness should be considered in the design and fabrication process to reach a final product with optimized mechanical integrity, desired target capacity of the inserted drug, robust extraction of signals, and the minimized pain by the patient. For example, a higher aspect ratio of needles can lead to a more convenient insertion, less pain, but weaker mechanical strength and integrity (Krieger et al., 2019; Mansor et al., 2019).

A diverse range of materials has been reported in the fabrication of MNs. These include polymers, metals, and inorganic materials (Ali et al., 2020; Bhatnagar et al., 2019; Gholami et al., 2019; Zhu et al., 2020a). Although the group of inorganics, such as glass, silicon, and ceramics, and a group of metals, including titanium and aluminum, were initially used for the fabrication of MNs, recently polymers and hydrogels have been of higher interest because of the need for biodegradable and dissolvable MNs. Polymeric MNs have become feasible by advances in polymer science and the emergence of new fabrication tools such as 3D printing (Bhatnagar et al., 2019). Table 1 shows the typical materials used in 3D printing technologies.

Introduction to 3D printing technologies

Stereolithography (SLA), one of the earliest 3D printing technologies (Amin et al., 2016a), works based on photochemical processes in which, using UV light and a digital micromirror device, a photocurable liquid polymer is cured in a layer-by-layer process to shape the product (Amin et al., 2016a; Ghaderinezhad et al., 2020; Quan et al., 2020; Yenilmez et al., 2016b). Digital light processing (DLP) is another 3D printing technology, similar to SLA, which uses several mirrors along with a lightbulb, instead of UV light, to cure the

Table 1. Most common additive manufacturing methods, used material, spatial resolution, advantages, and drawbacks of each

Method	Typical materials	Resolution	Advantages	Drawbacks
Stereolithography (SLA)	Resins with photo-active monomers acrylates – epoxides (Ligon et al., 2017) - DC 100 (high accuracy) - DC 500 - DL 350/360 (high flexibility) - AB 001 - GM 08 (high flexibility) - DM 210 - DM 220	10 μm (Ngo et al., 2018)	Fine spatial resolution - high quality (Ngo et al., 2018) - good surface quality - good precision (Ligon et al., 2017)	Supports limited materials - slow printing - expensive (Ngo et al., 2018) - poor biocompatibility - limited mechanical properties (Ligon et al., 2017)
Digital light processing (DLP) (Ligon et al., 2017)	Acrylates - epoxides - plas range (High resolution and chemically resistant) - superCAST - superWAX	25–100 μm	High printing accuracy - low cost - shorter build time than SLA - less affected by oxygen inhibition compared to SLA - better surface quality - low initial vat volume is needed	Limited mechanical properties
Continuous liquid interphase printing (CLIP) (Ligon et al., 2017)	Acrylates - rigid polyurethane (RPU) - flexible polyurethane (EPU) (impact resistant) - elastomeric polyurethane - cyanate ester (CE) - prototyping (PR) -	75 μm	Higher build speed than DLP	Low viscosity resin is needed
Two/multi-photon polymerization (TPP/MPP) (Ligon et al., 2017)	Acrylates	100 nm - 5 μm	High spatial resolution	Low build speed - limited material
Powder-bed based methods (selective laser sintering (SLS) - selective laser melting (SLM))	Compact fine powder metals - alloys and limited polymers (Ngo et al., 2018) - PA12 – PEEK (Ligon et al., 2017) titanium (biocompatible) - stainless steel - aluminum - cobalt/chrome – nickel-based alloys	50–250 μm (Ligon et al., 2017)	Fine resolution - high quality - durable - large surface area, good for scaffolds of tissue engineering - good mechanical properties (SLM) - less anisotropy (Ligon et al., 2017)	Slow printing - expensive - porosity - lower mechanical properties due to the porous structure (SLS) - high power supply - high printing temp - rough surface - poor reusability of unsintered powder (Ligon et al., 2017)

(*Continued on next page*)

Table 1. *Continued*

Method	Typical materials	Resolution	Advantages	Drawbacks
Fused deposition modeling (FDM)	Continuous filament of thermoplastic polymers - continuous fiber-reinforced polymers (Ngo et al., 2018) – PLA (Ligon et al., 2017) - ABS - ASA - Nylon 12 - PC - PPSF/ PPSU - PEI or ULTEM (Biocompatible) - PLA – TPU	50–200 μm (Ngo et al., 2018)	Low cost - high speed – simplicity (Ngo et al., 2018)	Weak mechanical properties - limited material (thermoplastics) – layer-by-layer finish (Ngo et al., 2018) - rough surface - high temperature during the extrusion process (incompatible for cells) (Ligon et al., 2017)
3D dispensing (Ligon et al., 2017)	Thermoplastics - photoresins - composites - hydrogels - biomaterials	100 μm - 1cm	Wide range of materials	Rough surface - narrow viscosity process window
3D printing (Binder jetting) (Ligon et al., 2017)	Stretch - PLA - ceramics	100 μm	Fast - allow multi-material AM	Rough surface - limited strength of parts
Inkjet printing (Ngo et al., 2018)	A concentrated dispersion of particles in a liquid (Ink or paste)	5–200 μm	Quick printing	Weak adhesion between layers
PolyJet (Ligon et al., 2017)	Acrylates - VeroWhite Plus - digital ABS - FullCure RGD 720 - Rigur RGD 450 - biocompatible material	25 μm	Fast - allow multimaterial AM	Low viscosity ink is needed
Direct energy deposition (DED) (Ngo et al., 2018)	Metals and alloys in the form of powder or wire ceramics and polymers	250 μm	Reduced manufacturing time and cost - good mechanical properties - accurate composition control - good for repair and retrofitting	Low accuracy - low surface quality - dense support structure is needed - limitation in printing complex shapes

photopolymer to shape the final structure (Zhang et al., 2020). In addition, curing in the SLA method is in a point-to-point manner, whereas in DLP each layer is cured at once (Ligon et al., 2017; Zhang et al., 2020).

Multiphoton polymerization (MPP) is another method of 3D printing, featuring high resolution for the fabrication of structures in submicron scales. An MPP 3D printer consists of an femtosecond laser (fs) laser and pairs of laser scanners. By focusing the laser beam to a highly restricted region, the nonlinear absorption of two or more photons by polymers solidifies the photoresist in the exposed regions (Geng et al., 2019). Two-photon polymerization (TPP) lithography, also called 3D direct laser printing (Lightman et al., 2017) and direct laser writing (DLW) (Gissibl et al., 2016; Ligon et al., 2017), employs fs laser pulses and simultaneous absorption of photons to cure the material. In this method, the laser's focal point can be directed in all directions unlike the SLA and DLP technologies, in which the curing occurs layer by layer (Lee et al., 2007).

Fused deposition modeling (FDM) 3D printers melt a thermoplastic filament and extrude it through a nozzle on the build platform to shape a layer of the structure (Knowlton et al., 2015b, 2017a). FDM allows the usage of different filaments in a single process. For instance, the filament of the main structure can vary

from the filament used for the fabrication of the supporting structures, making the post-processing of the product easier. After cooling down and solidification of the deposited layer, the next layer is fabricated by repeating the process, leading to the formation of the final product (Dhinakaran et al., 2020).

Co-axial extrusion is another 3D printing technology mainly used for bioprinting and fabrication of cell-laden structures. Although the process for this method is similar to extrusion-based printers, there are two material feeders for co-axial extrusion 3D printers, in which one of the materials is printed as a coating on the other one (Liu et al., 2018).

The principle of selective laser sintering (SLS) 3D printers is based on utilizing a laser beam, as a concentrated heating beam, to sinter tightly compact thermoplastic powder in a build tank. Sintering means the process of heating powder particles so that particles can stick together, without reaching the melting point of the powder, to form a solid structure (Mazzoli, 2013). After the sintering of each layer, the new powder is loaded into the build tank and the process is carried out repeatedly to shape the final structure (Lepowsky and Tasoglu, 2018). Selective laser melting (SLM) uses a similar 3D printing technique to SLS, whereas SLM needs support structures, and metal powder is usually used. By reiterating laser and dot matrix data patterns, each layer solidifies, leading to the final product. Electron beam melting (EBM) is also used for 3D printing of metallic materials with a similar method to laser melting, except that the beams of electrons perform the melting instead of laser light (Amin et al., 2016a).

Material jetting is another 3D printing method that shapes the object and supporting structures by jetting the material onto the build platform, in a layer-by-layer process, using inkjet print heads to shape the product. Photopolymer jetting is also an analogous process in which the layers of liquid photopolymer are jetted onto the build platform, followed by a UV light curation. Similar to material jetting, inkjet print heads are used in the binder jetting technique. However, in this method, a liquid adhesive is jetted onto the layers of powder in the build tank. By feeding new powder, the next layers are created successively, leading to the final product. Unlike material jetting, no support structures are needed for the fabrication of complex designs by binder jetting (Amin et al., 2016a). Table 1 illustrates the advantages and disadvantages of each technology and the printing resolution each method offers.

There are various tradeoffs and limitations of 3D printing techniques that have to be considered in the design iteration and prototyping stage of MN fabrication. To avoid fracture and perilous leftovers in the skin during insertion, physiologically relevant mechanical properties such as the compliance of elastic moduli between skin and MN are desired. Powder-bed-based methods (e.g., SLS and SLM) offer fine mechanical properties because metallic alloys (e.g., stainless steel, nickel, aluminum, and titanium) can be used. However, the biocompatibility of metal alloys or their compliance with biocompatible coatings should be considered before proceeding with the fabrication method. Moreover, MNs fabricated by powder-based methods possess undesired rough surfaces. In addition, the high temperature of the sintering process confines the use of biological material (e.g., cells). Overall, taking into account the smallest attainable size features, powder-bed-based methods are not practical for the production of MNs. Extrusion-based methods (e.g., FDM) are simple, cost-effective techniques that can operate with biocompatible materials. However, the final resolution of this approach is lower than that of vat polymerization methods. Furthermore, low mechanical properties, layer-by-layer finish of the surface, and high temperature utilized in the process pose challenges against the implementation of extrusion methods for MN fabrication. Vat polymerization techniques have attracted more attention for the fabrication of MNs compared with other 3D printing methods. All vat polymerization methods offer a relatively high resolution (Table 1). The selection of the fabrication method should be based on the proposed application. For instance, MPP has the highest resolution, whereas the process is quite slow and supports limited materials. Therefore, MPP may be considered as a suitable method for prototyping and research applications rather than mass production. Likewise, DLP is a faster method, which is less affected by oxygen inhibition compared with SLA, whereas SLA has a higher resolution.

3D printing technologies in fabrication of MNs

SLA, DLP, MPP methods, and photopolymer jetting are of high interest for the fabrication of MNs due to the higher resolution and wide material choice offered by these methods. SLA, for instance, was used for the fabrication of poly(propylene fumarate) (PPF) MNs in a dynamic mask projection microstereolithography (μSLA) setup. The fabricated MNs had 1,000 μm height, 200 μm base diameter, and 20 μm apex

diameter (Lu et al., 2015). Also, the SLA 3D printer, with a z axis resolution of 25 μm and x axis resolution of 140 μm, was employed to fabricate biocompatible polymeric MNs and then insulin solutions were deposited on the needles using inkjet printing (Pere et al., 2018). In another case, SLA 3D printing was used for the fabrication of 1,000 μm height cross-shaped polymeric MNs, followed by coating chemotherapy medication (cisplatin) formulations on the needles, via inkjet printing, for skin cancer treatment (Uddin et al., 2020). DLP was utilized to produce MNAs on personalized curved surfaces using castable resin, post cured to cure any remaining uncured resin for 2 h. Using this 3D printing method, with XY resolution as well as a printing layer height of 50 μm, 300 μm base diameter, and 900 μm height were obtained for MNAs (Lim et al., 2017). TPP lithography was utilized to produce cylindrical, pyramidal, and conical biocompatible magnetic MNs, using drop cast IP-DIP resist, on a single-side polished silicon wafer. MNs fabricated by TPP had a base diameter of 630 nm, aspect ratio of 1:10, pitch of 12 μm, and coated by a 120-nm thickness iron coating (Kavaldzhiev et al., 2017). Also, TPP lithography 3D printing was employed to fabricate MNs, with IP-S (Nanoscribe GmbH) photoresist, for performing perforations on the scale of millimeters. MNs had a shaft diameter of 100 μm, a height of 350 μm, and a taper angle of 60° (Chiang et al., 2020). In another study, the TPP 3D printing method enabled the fabrication of hollow MNs using IP-S photoresist, with an outer tip diameter of 50 μm, an inner diameter of 30 μm, tapered angle of 5°, and height of 200 μm (Moussi et al., 2020). In another study, an extrusion-based 3D printer with two nozzles was used to produce patches of MNs for drug delivery (Wu et al., 2020). One of the nozzles of the printer is used to extrude substrate material, whereas the other nozzle prints the material that contains the drug to form the cylindrical shape of the MNs. The achieved resolutions reported in this study were 601 μm for base diameter, 24 μm for tip diameter, and 643 μm for height.

Additive manufacturing can be used to fabricate MNs by directly 3D printing MNs or by producing female master molds. Mold-based techniques are suitable for the mass production of MNs with a diversity of materials such as biocompatible hydrogels (Tejavibulya et al., 2019). Nonetheless, to make any changes in the dimensions of MNs, the entire process of design and fabrication of mold should be repeated. An SLA-based two-step "print and fill" method was developed (Krieger et al., 2019) for fabricating customizable replica molds (Figure 3). Firstly, the MNA master was printed using an SLA 3D printer. Subsequently, a UV-curable resin was used to obtain the desired MN length. Finally, a silicon female master mold was produced using the 3D-printed MNA master (Krieger et al., 2019). UV curable resin was used to produce MNs with different aspect ratios (3:1, 4:1, and 5:1) and layer heights (25, 50, 100 μm) to determine the discrepancy between the desired and resulted height, needle's tip angle, and tip ratios (Figure 4). Despite changing design features, the tip radii of MNs were at the range of 20–40 μm. Furthermore, higher printing layer heights result in faster printing, while yielding lower surface quality (Krieger et al., 2019; Yao et al., 2020). Two-photon polymerization with a 780 nm light wavelength was used to produce soft elastomeric MN replica molds. Using these molds, MNs with 700 μm height and 150 μm shaft diameter were fabricated (Rad et al., 2017). 3D direct laser printing along with micromolding was employed to fabricate undercut MNs (Balmert et al., 2020). The 3D-printed master MNA was used to generate replicas that were organized on a 3D-printed photosensitive resin holder. Using this holder, a production mold was fabricated with polydimethylsiloxane, which enabled the fabrication of multiple MNAs at once (Figure 5). Although micromolding is a suitable method for large-scale production, disassembling MN with an undercut is complex and susceptible to failure. Using micromolding and flexible production molds not only addressed the disassembling problem but also the production molds can be used several times, which reduced the fabrication cost of MNAs (Balmert et al., 2020). In another study, drawing lithography was used to fabricate MN molds using UV-curable resin (Lin et al., 2016). This method is faster and less costly compared with photolithography and etching techniques. However, the main drawbacks of drawing lithography approach are low control over the geometry of MNs and incapability to produce different MN profiles (e.g., cylindrical and pyramidical) (Lin et al., 2016).

One of the impediments of achieving desired geometrical factors is the restricted resolution of the employed fabrication method. Although several studies have been conducted to enhance the resolution of 3D printers by modifying the printer itself (Gong et al., 2020; Johnson and Procopio, 2019; Serex et al., 2018), integrating 3D printing with other techniques can enhance the resolution of the final MN without manipulating the printer. To overcome the resolution limit of 3D printers, the SLA 3D printing technique was integrated with shrinkable hydrogels (Ochoa et al., 2015). MNs with tips down to 9.6 μm radius of curvature were fabricated. The resolution of MNs produced with this method was higher than MNs printed with the same 3D printer without utilizing shrinkable hydrogel.

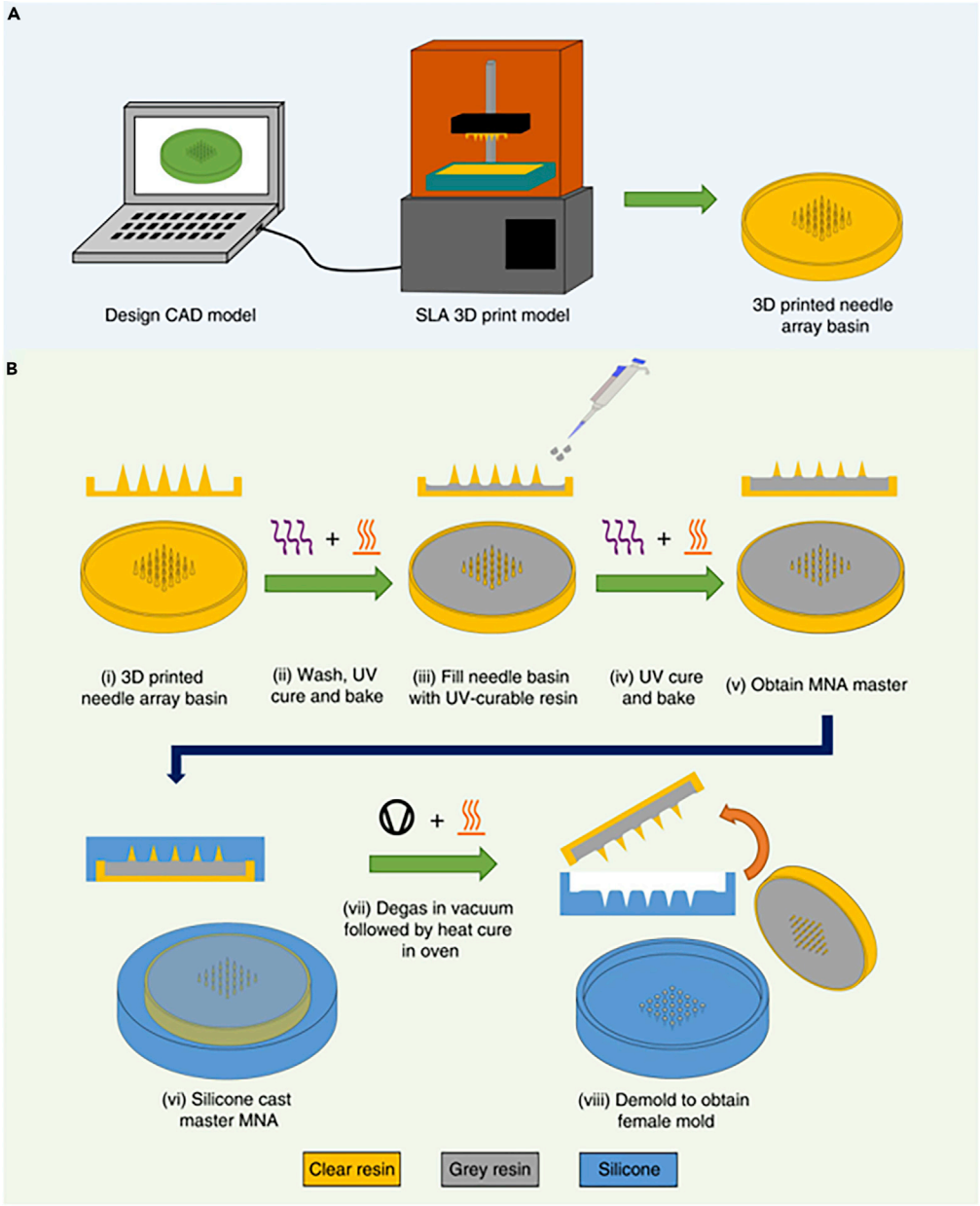

Figure 3. Step-by-step illustration of fabricating microneedles (MNs) with stereolithography (SLA) 3D printing and replica mold method

(A) The design procedure was followed by 3D printing of the designed structure using an SLA printer.

(B) The 3D-printed MNs were washed and then cured with UV light, followed by filling the basin with UV-curable resin to obtain the desired MN height, resulting in a microneedle arrays (MNA) master. In the next step, using silicone, degassing by the vacuum chamber, and heat curing in the oven, the final female master mold can be produced (Krieger et al., 2019). Adapted with permission from (Krieger et al., 2019). Copyright 2019, Springer Nature.

3D printing with programmed shape deformation, also known as 4D printing, is one of the approaches to produce bioinspired MNs with curved barbs (Han et al., 2020), increasing the adhesion of MNs to the tissue by 18 times (Morde, 2018). Using μSLA, MNs with a base diameter of 400 μm, length of 4 mm, and cone tip angle of 10° were fabricated. The barbs possess a 200 μm base diameter with 450 μm length. Sudan I as a photoabsorber (PA), poly(ethylene glycol) diacrylate, phenylbis (2,4,6-trimethylbenzoyl) phosphine oxide as a photoinitiator (PI), and Mn ≈ 250 (PEGDA 250) as a monomer were used to produce MNs with curved barbs (Han et al., 2020). One of the issues that adversely affects the surface quality of 3D-printed MNs is the

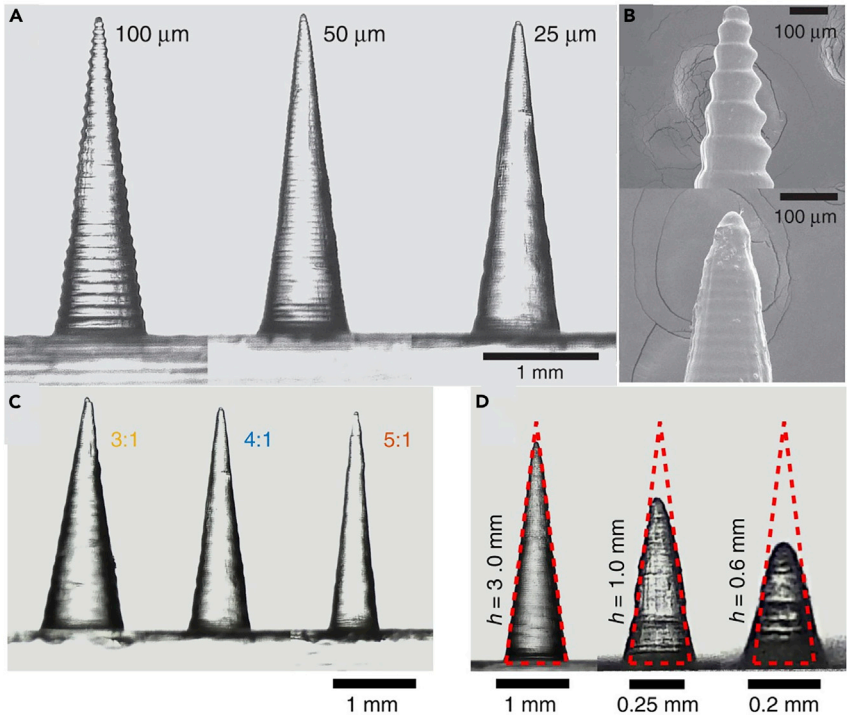

Figure 4. Scanning electron microscope (SEM) images of microneedles (MNs), fabricated by stereolithography (SLA), with different feature sizes

(A) Fabricated MNs via various printing layer heights: 100, 50, and 25 micrometers. Although lower layer heights bring about better surface quality, the printing process will be slower. Hence, choosing the proper layer height is a trade-off between surface quality and time.

(B) Tip of fabricated MNs (top:100 µm, bottom: 25 µm layer height).

(C) Different aspect ratios. A higher aspect ratio here means a gradual increase of shaft thickness that results in a painless insertion of MN. However, thinner needles possess low mechanical strength that can result in breaking the needle in the insertion process.

(D) The discrepancy between the input and output height. Higher aspect ratios suffer more from discrepancy issues (Krieger et al., 2019). Adapted with permission from (Krieger et al., 2019). Copyright 2019, Springer Nature.

layer-by-layer nature of the 3D printing process. To solve this limitation, continuous liquid interface production (CLIP), a single-step, based on vat polymerization, continuous AM method was devised to prototype MNs rapidly (Caudill et al., 2018; Johnson et al., 2016). Using polyacrylic acid, trimethylolpropane triacrylate, and photopolymerizable derivatives of polyethylene glycol as well as polycaprolactone, MNs with 1,000 µm height, 333 µm base width, and 2.3 µm tip radius were produced by CLIP (Johnson et al., 2016). Furthermore, magnetorheological drawing lithography (MRDL) AM method, which needs no masks and molds, has been introduced (Chen et al., 2018, 2019c) for fabricating flexible MNAs (Ren et al., 2017). To achieve cost-effective rapid mass production, droplets of the polymerized mix of epoxy novolac resin with iron microparticles on a polyimide substrate were drawn, assisted by a magnetic field, to form liquid MNAs, which were solidified by applying hot air and vacuuming. MNs with a height of 600 µm and a tip radius of 12 µm were produced with this method. Finally, a coating of the Ti-Au film was applied to the MNAs to ensure compatibility and conductivity (Figure 6).

There have been attempts to fabricate even smaller needles. Nanoneedles (NNs) have been fabricated by optical vortex pulses, confined laser spinning (CLS), and metal-assisted chemical etching. Each of these fabrication methods offers pros and cons. Etching, for instance, is not a suitable method for producing NNs made of hard metals (e.g., gold, silver). In this regard, femtosecond DLW was used to produce different sizes of NNs by controlling laser pulse energy with a combination of half-wave plates and Brewster polarizer (Yendeti and Soma, 2020). Because no chemicals were involved in the fabrication process, this approach was considered an environmentally friendly method. Microscope objectives (20× and 60× lenses) were examined to focus laser pulses, which resulted in producing NNs with higher packing densities

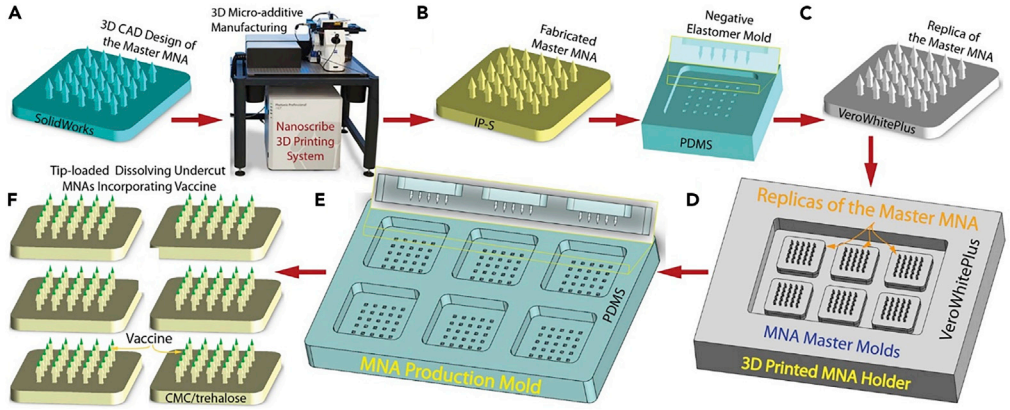

Figure 5. Scalable microneedle array (MNA) fabrication in six steps, using 3D direct laser printing and molding

(A) 3D design of size features of the MNA, based on the proposed application.

(B) Direct production of designed MNA using 3D direct laser printing. MNs with a height of 750 μm, base diameter of 150 μm, arrow base radius of 250 μm, and a tip angle of 30° were produced.

(C) Replicating the master MNA mold with high fidelity by a two-step micromolding process.

(D) Arranging multiple MNA master molds on a 3D printed holder.

(E) Production of MNA fabrication molds by polydimethylsiloxane (PDMS).

(F) Loading the desired drug on the tip of the fabricated MNAs by a spin-casting method (Balmert et al., 2020). Adapted with permission from (Balmert et al., 2020). Copyright 2020, Elsevier.

using 60× lenses. However, NNs fabricated by 60× lens had poor bonding with glass coverslip compared with that of the 20× lens. In an LDW process to fabricate NNs, carried out by evaporating metal, the laser focuses on a certain spot where the center of the laser beam that has higher intensity (Gaussian distribution) increases the temperature above the evaporation temperature of the metal. On the other hand, the edges of the laser beam with lower intensity raises the temperature above the melting temperature and below the evaporation temperature of the material. Thus, when the evaporated metal at the center wants to expand and escape with high pressure, it expels the melted metal at the edges and forms NNs.

EMERGING APPLICATIONS IN BIOMEDICAL ENGINEERING

Drug delivery

MN patches have applications in immunology, cosmetics, diagnostics (Yang et al., 2019), and continuous and constant release of therapeutic agents through the skin after topical treatment (Kim et al., 2019). Generally, there are a few facile tailored systems to deliver specific molecules into the body. The presence of immunologically active cells, namely antigen-presenting cells (APCs), allows the skin to be an active immune organ. Hence, delivering drugs through the skin is more efficient and durable than intramuscular delivery owing to the presence of fewer immuno-cells in muscles than skin (Lambert and Laurent, 2008). However, delivering drugs through the skin has not been developed to its full potential due to the shortage of minimally invasive, efficacious, user-friendly, and ubiquitous technologies (Kabashima et al., 2019). Drug delivery through the skin can obviate the need for conventional intramuscular injections. The disadvantages of conventional needles are fear of needles (trypanophobia), complex transport and storing requirements, contamination, the possibility of disease transmission, demanding trained personnel to perform vaccination, chance of injuries, and pain brought about by needles (Norman et al., 2014; Prausnitz, 2004; Prausnitz and Langer, 2008). MN patches deliver target biomolecules to the local area under the administration site or send bioactive compounds to the remote sites through the circulatory system (Figure 1A). In clinical settings, the local delivery of certain chemicals, factors, and drugs could be achieved via intradermal, subcutaneous, and intramuscular approaches (Yang et al., 2019). The direct injection of target molecules to the muscles and subcutaneous tissue facilitates the passive diffusion of the drug to the systemic blood system. A major challenge in the application of MNs is to release the target molecules via the cutaneous barrier (Indermun et al., 2014). In the delivery of target molecules, the cutaneous tissue is temporarily disrupted after piercing the stratum corneum to bypass the hydrophobic layer and beneath viable keratinocytes. In most cases, target molecules placed in the epidermis or upper dermis reach systemic circulation through passive diffusion. Therefore, MN patches are candidates for painless and self-administrated hypodermal and dermal injection (Baek et al., 2017).

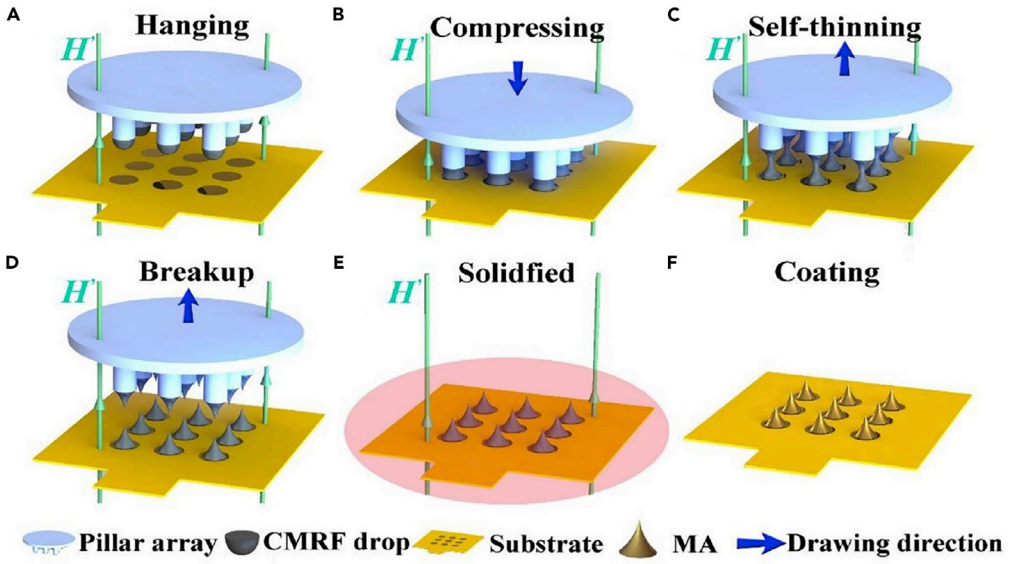

Figure 6. Sequential steps of microneedles (MNs) fabrication by magneto-rheological drawing lithography (MRDL), an additive manufacturing method

(A) Pillar tips, with a diameter of 700 μm, were coated by dipping in curable magnetorheological fluid (CMRF).

(B) Then, the pillars were moved downward, toward a substrate, with a constant speed of 1.5 mm/s to press droplets to the substrate for 1 s.

(C) Pillars moved upward with the speed of 1.5 mm/s and stopped in 12 mm from the substrate, resulting in a necking effect.

(D and E) When the thinned CMRF lines broke up at room temperature, the MNs were solidified at 100°C for 1 h.

(F) Subsequently, the fabricated MNs were coated by titanium (Ti) and gold (Au) using a magnetron sputtering machine (Ren et al., 2017). Adapted with permission from (Ren et al., 2017). Copyright 2017, Elsevier.

Polymer MNs were developed by μSLA 3D printing with programmed deformation (4D printing) to study their adhesive properties in the cutaneous system for application in biosensors and long-term monitoring and delivery systems (Han et al., 2020). The fabricated MNs included curved barbs to improve adhesion capacity. By tuning the curving thickness, angle, and material composition, the adhesion of MNs with barbs to the tissue was increased by 18 times compared with a needle without barbs (Morde, 2018). The fabricated MNAs were tested to deliver a drug in an *ex vivo* chicken tissue (Han et al., 2020).

MNs were integrated with microfluidic channels including multiple inlets (Yeung et al., 2019). Using a biocompatible and transparent resin based on methacrylic acid esters as the building material, SLA 3D printing allowed rapid cost-efficient fabrication of 12 devices in 2.5 h. The integrated microfluidic chamber was designed as a hydrodynamic mixer of fluids, which enabled transdermal drug delivery. Different parameters and geometries were tuned to achieve an optimized performance, including a high aspect ratio needle tip. The optimal radii of curvature of MNs were as low as 25 μm, in +45° printing orientation, with a base width of 800 μm and a central bore of 600 μm. The device was tested in an *ex vivo* porcine skin (Figure 7). SLA 3D printing has been also utilized to fabricate MNAs with a biocompatible photopolymer, class I resin, Dental SG, by Formlabs, coated by insulin and drug carriers on the needles using inkjet printing (Economidou et al., 2019). The 3D printer has a resolution of 25 μm on the z axis and 140 μm on the x axis, resulting in MNs with a height of 1 mm and tip size of 100 μm. The fabricated MNA was tested on *in vitro* porcine cutaneous tissue. The needle was designed in two shapes of a pyramid (1 × 1 × 1 mm) and a spear (0.08 × 1 × 1 mm), in which the geometry of the pyramid needed a lower force to penetrate the skin and reach deeper layers. Xylitol had the optimum performance as the drug carrier in the system. *In vivo* testing in a diabetic mouse model showed that insulin lowered the glucose level in the blood within 60 min. In another study, the same method, material, and coating technique was used to fabricate cone shape MNs to study the effect of MN shape on delivery time as well as the required force for insertion (Pere et al., 2018). The device was tested *in vitro* porcine skin, in which insulin was released within 30 min. Among the drug carriers used, xylitol showed the optimal result. Although the needle design did not affect the delivery time, the cone shape needed lower applied force for penetrating the skin as

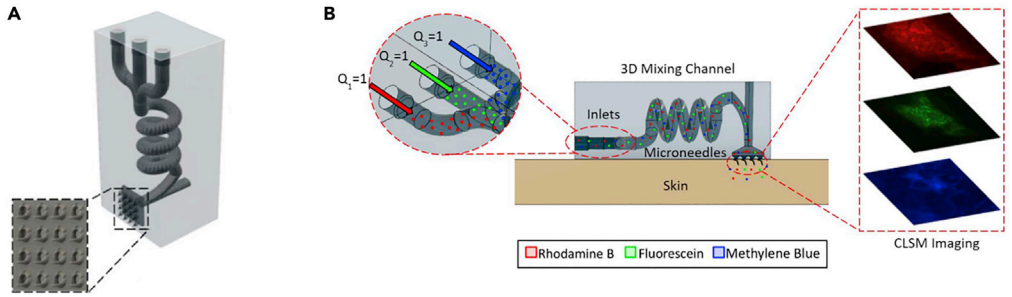

Figure 7. The integration of microfluidic devices with microneedles offers better fluid management abilities, resulting in a more advanced level of controlled drug delivery

(A) An illustration of the proposed device fabricated by stereolithography 3D printing, with three separate microfluidic inlets and microneedles (MN) as the outlet. The zoomed section shows the MNs.

(B) *Ex vivo* transdermal delivery of three model drugs, from multiple inlets, into a porcine skin (Yeung et al., 2019). Adapted with permission from (Yeung et al., 2019). Copyright 2019, American Institute of Physics.

compared with the pyramid pattern. In another case, the SLA 3D printing technology was used in the fabrication of MNAs with a polymer resin (Xenikakis et al., 2019). The printed needle height was shorter than the CAD model because of the solidification shrinkage. The tip radius was set to the best resolution of the SLA printer, 50 μm. Although MN heights of 1,090, 875, 470 μm were printed, only the 875 μm MN was suitable for clinical tests, because 1,090 μm MN can cause pain by reaching the nerve system, whereas 470 μm was not efficient due to its short length. Mechanical property analysis indicated reasonable strength in the fabricated MNAs against fracture in high forces. Employing Finite Element Analysis, the force required for the needle to penetrate the skin was calculated. This estimation met the experimental amount when the fabricated MNAs were tested on human skin *in vitro*. Transdermal delivery and permeation of two model dyes were also tested, demonstrating satisfactory penetration and higher cumulative amount in both cases after treating with the MNs.

Using 3D laser lithography (also known as DLW) and micromolding, a scalable manufacturing method was developed for the fabrication of soluble undercut MNAs for drug delivery (Balmert et al., 2020). The MNs were fabricated by CMC/trehalose hydrogel, prepared by dissolving a mixture of sodium carboxymethylcellulose (CMC) and D-(+)-trehalose dihydrate, at a total solute concentration of 30% w/w in endotoxin-free water. Soluble MNAs were rigid enough to endure the penetration process in a dry state. Right after insertion, MNs dissolve into the skin rapidly. Undercutting MNAs allow retention of the MNs in the skin as well as in the non-cutaneous tissues. This device may be utilized for either intradermal or non-cutaneous drug delivery (e.g., cardiac and liver tissues). To evaluate the performance of a dissolving MNA, penetration, solubility, and efficiency of delivery should be considered. Ten minutes of MN insertion into living human skin explant resulted in 80% drug delivery, where increasing insertion duration to 20 min did not substantially amplify the delivery rate. MNs had a height of 750 μm, an apex angle of 30°, stem width of 150 μm, and arrow base width of 250 μm.

TPP 3D printing technique, with 780 nm wavelength, was used to fabricate high-quality master templates of MN arrays using polylactic acid (PLA) and silicone elastomer mix. Two types of MNs were developed in this study: first, dissolving MNs (DMNs), which were efficacious in the delivery of both hydrophilic and hydrophobic drugs; second, hydrogel-forming MNs (HFMNs), which were useful in interstitial fluid extraction from the body and delivery of drug molecules. Different designs (e.g., conical and pyramidal MNs), needle sizes, the spacing between needles, and needle density were examined to find the optimum features to achieve the most optimum mechanical properties as well as drug delivery efficiency. Longer MNs possess a more efficient drug deposition rate, due to the deeper penetration into skin, with lower mechanical strength. In addition, by increasing the interspacing of MNs, although, because of the reduced number of MNs per array, the overall amount of delivered drug decreases, the drug delivery efficiency improves (Cordeiro et al., 2020). Besides the delivery of the substances to the treatment area, it is important to penetrate MN without damaging the surroundings in the sensitive organs. One of the challenging examples is the safe and precise delivery of therapeutics to the inner area of the ear to treat hearing diseases. MNs have been employed to delicately perforate the round window membrane, one of the two openings from the middle ear to the inner ear (Aksit et al., 2018). Using TPP lithography 3D printing, MNs with a tip radius

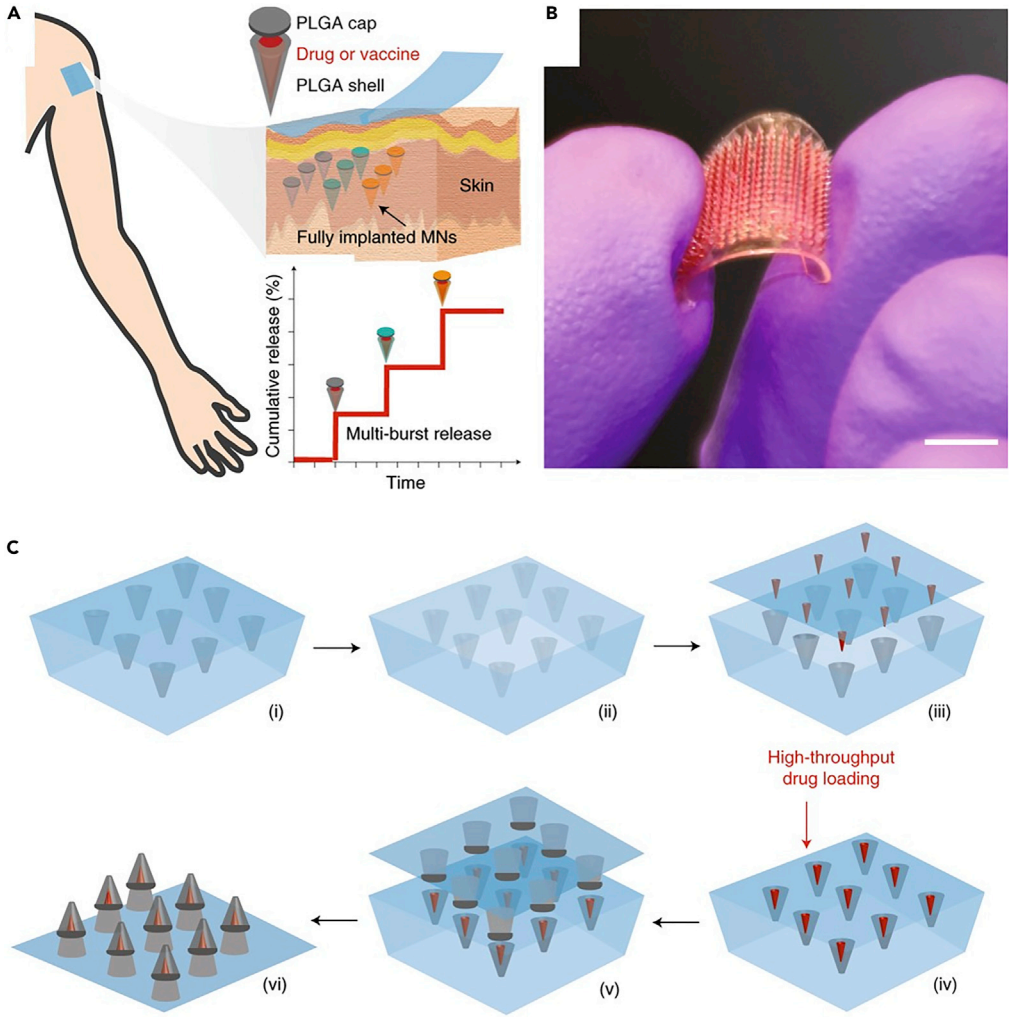

Figure 8. MNs with a core-shell structure featuring programmable drug-releasing kinetics with a one-time insertion mimicking the multi-injection drug or vaccine delivery systems

(A) Schematic view of the three constituent elements of the fabricated MNs: shell, cap, and drug core, demonstrating the underlying principle of the kinetics of controlled drug delivery.

(B) Optical image of the fabricated MNs. Scale bar: 0.5 cm.

(C) Step-by-step 3D manufacturing process of MNs: (1) a PDMS negative mold of MNs was filled with PLGA; (2) a positive polylactide (PLA) mold was used to encroach the MNs inside the PDMS mold; (3 and 4) arrays of drug cores were aligned and loaded into MNs in a high-throughput drug-loading process; (v) PLA supporting patch including the cap layer was attached to the MNs in a heat-sintering process. (vi) The MNs were ready after peeling off the PDMS mold (Tran et al., 2020). Adapted with permission from (Tran et al., 2020). Copyright 2020, Springer Nature.

of 500 nm, a height of 200 μm, and a shank radius of 50 μm were fabricated using IP-S photoresist. The MN was used to perforate the round window membrane of a guinea pig ear *in vitro*. Although the membrane was not torn, a separation in the fibers of the membrane was reported because of the fiber-to-fiber decohesion.

One of the challenges of vaccination is the need for the repetition of vaccination with a specific time interval, which imposes further expenses and agitates patients. One-off administration systems are a preferable replacement for applications that requires multiple injections, such as cancer therapeutics or growth hormones (Tran et al., 2020). MNs, with a core-shell structure, were fabricated using TPP (for silicon wafer patterning) and photolithography (for the fabrication of molds for the MN caps and the supporting array), followed by a 3D manufacturing process to assemble the shell and the cap of the MN along with a drug core

(Figure 8), enabling programmable drug-releasing kinetics with time intervals (Tran et al., 2020). Each MN had a height of 600 μm, a core height of 400 μm, a base diameter of 300 μm, and a core diameter of 200 μm. Modifying the degradation of the shell, which was made of poly(D,L-lactide-*co*-glycolide) (PLGA), a biodegradable polymer, provided the ability to control the release time of the drug. Using this approach, with only one-time insertion, vaccine antigens can be controllably released over defined periods of time, which was tested for Prevnar-13 vaccine on rats (Tran et al., 2020).

An extrusion-based 3D printer with 2 nozzles was used to produce patches of MNs with 643 μm height and 24 μm tip diameter for insulin delivery (Wu et al., 2020). Following the insertion of insulin-loaded MNs to the skin of mice with type 1 diabetes, after ~1 h, the blood glucose concentration decreased to the normoglycemic range, with no report of hypoglycemia during drug delivery. Moreover, the blood glucose concentration remained in the normoglycemic range up to 40 h after insertion, demonstrating the adequate drug delivery performance of the proposed MNs.

The treatment of cancers imposes substantial financial burdens on health systems worldwide (Semin et al., 2020). In cancer biology and therapy, most of the published data have focused on the stimulation of innate and adaptive immune cells by the introduction of specific antigens, genetic elements, and adjuvants or direct delivery of anticancer agents (either alone or in combination with nanoparticles) (Figure 9A) (Wang et al., 2016), and the use of conventional and novel approaches to deliver chemotherapeutic agents exhibited sub-optimal results in animal models or clinical settings (Jacinto et al., 2020). MN patches have applications in drug delivery in cancers and metabolic disorder diagnosis (Yang et al., 2019) by opening new avenues to support fast-acting sophisticated drug delivery with specified doses in a controlled manner (Queiroz et al., 2020). Moreover, efficient delivery of chemotherapeutic agents to the cancer growth sites while diminishing leakage to the systemic circulation as well as neighboring tissues and minimizing adverse side effects are of great importance (Mojeiko et al., 2019). In this regard, MN patch technology can allow the treatment of metabolic diseases by enabling patients to painlessly self-administer injections (Figure 9B) (Yang et al., 2019). Hence, the integration of advantages of 3D printing with the potency of MNs for controlled cancer drug delivery can increase the effectiveness of cancer diagnosis methods.

Sample extraction

Other applications of MNAs are in extracting and obtaining samples from patients for bioassays and monitoring setups (Zhu et al., 2020b). Self-monitoring of blood glucose (SMBG) is a simple way to control blood glucose by the patients to prevent adverse ramifications of prolonged hyperglycemia. However, the extraction of blood with conventional needles is painful, which causes reluctance in patients to collect blood samples regularly. MNAs as a minimally invasive and painless method can facilitate the development of point-of-care (POC) blood collection (Farhan et al., 2017; Vincze et al., 2004).

A hollow MNA was developed along with a paper-based colorimetric detection method to detect glucose concentrations ranging from 4 to 7 mM L-1 by eye (Nicholas et al., 2018). Using SLA 3D printing, an initial master mold was prepared to build a negative mold, which was used to fabricate 400-μm long hollow MNA. This device could absorb samples in 5 s for POC applications. MNs should be able to withstand 0.028 to 0.030 N during insertion-axial load applied by the user to penetrate into the skin (Olatunji et al., 2013). Therefore, the mechanical properties of MNs should be studied to avoid fracture. The strength of the MNA was evaluated using a 50 N load cell that pushed toward the MN at a rate of 0.01 mm s-1. The reported MN was stiff enough for application in POC diagnostics (Nicholas et al., 2018).

Based on the DLP 3D printing technology, a new setup was built with high precision to print in micro-scale, being utilized for fabrication of MNs with a photosensitive hydrogel, which was cured with different blue light (Yao et al., 2020). Alginate hydrogel (5 wt%), which is similar to human skin in terms of mechanical properties, was used as an artificial skin to study drug injection, extraction, and detection by the fabricated MNs. MNs were soaked in deionized (DI) water for 1 day, whereas the artificial skin was soaked in an RhB solution for the same duration, subsequently, MNs were inserted inside the skin. The integrated density of RhB inside the MNs reached more than 20 mg L^{-1} in 25 min, enabling the successful detection of drugs in the skin.

Using a 3D-printed master mold, porous polydimethylsiloxane (PDMS) MNs with 1,000 μm height were fabricated to extract PBS from an agarose gel-based skin phantom (Takeuchi et al., 2019). In another study,

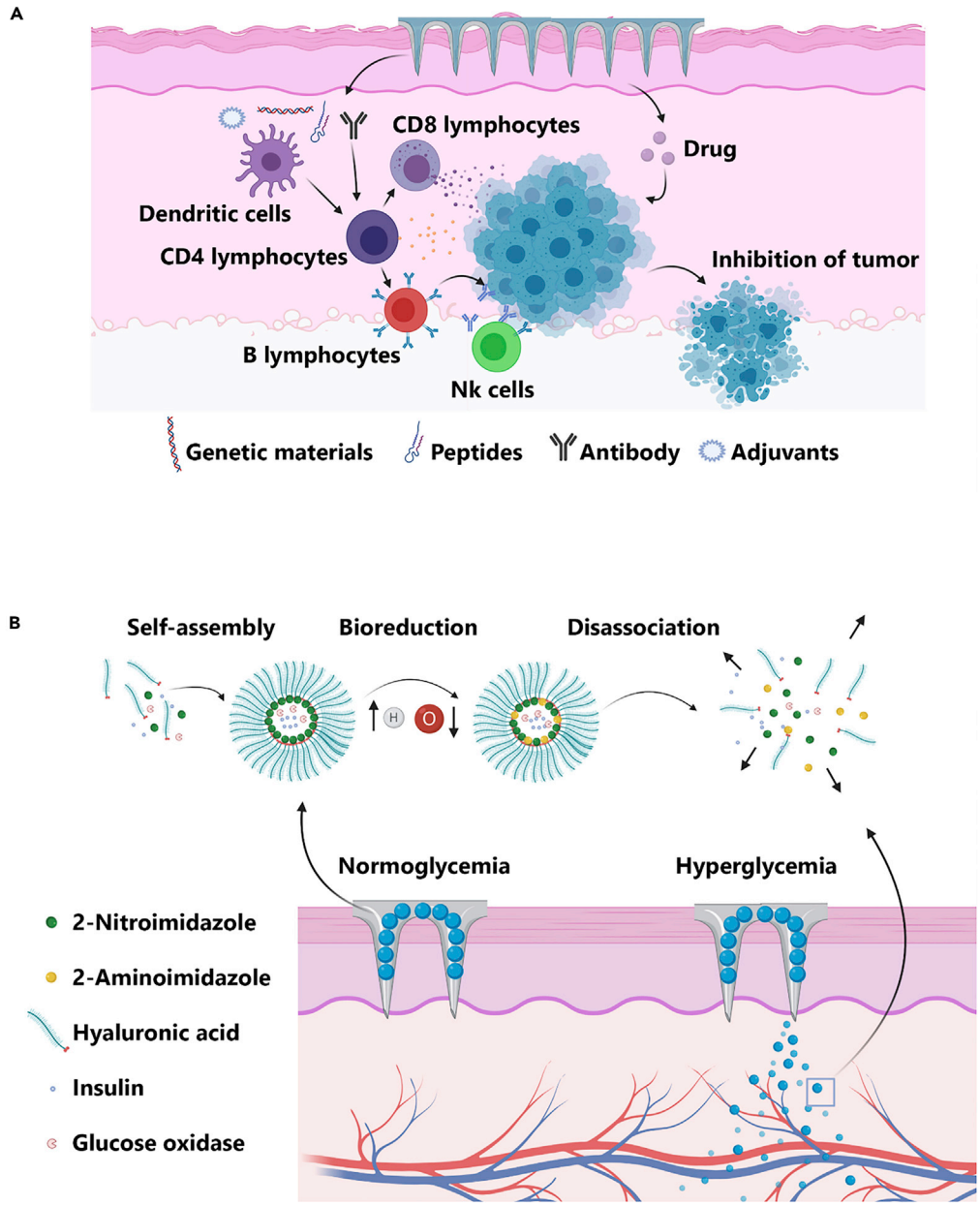

Figure 9. Application of the microneedle (MN) patches in cancer therapy

(A) The integration of antibodies, adjuvants, peptides, and genetic elements is done to stimulate immune cells and increase tumoricidal outcome along with chemotherapy.

(B) Intelligent needle structures are used to control the systemic levels of endocrine hormones upon the onset of metabolic diseases.

drawing lithography, an additive manufacturing method, was used to fabricate a hollow metallic MN for blood sample extraction (Li et al., 2013). Following an examination of various size features and resist thicknesses, a 1,800-μm height MN with a bevel angle of 15°, an inner diameter of 60 μm, and an outer diameter of 120 μm was the most efficient MN for blood extraction (Li et al., 2013).

To study the extraction of interstitial fluid from the skin, MN holders were prepared, using photopolymer jetting 3D printing technology, with flat, concave, convex, and bevel profile geometries in order to test the influence of MN holder on fluid extraction efficiency (Taylor et al., 2020). Ultra-fine needles were attached to

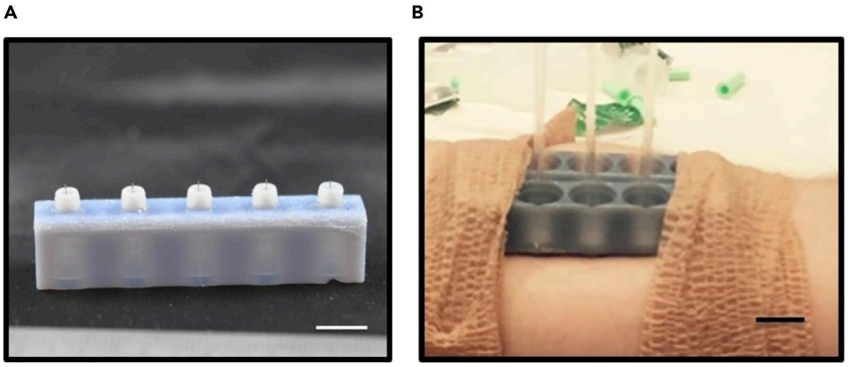

Figure 10. Microneedle arrays (MNAs) comprised of 3D-printed holder arrays and ultra-fine needles for dermal interstitial fluid extraction

(A) 3D-printed MN holder with attached needles, coated with a silicone lubricant to lessen the insertion pain (scale bar: 1 cm). MN holders not only do affect the extraction rate by applying pressure on the surroundings of the insertion site but they also protect the fragile MN during the insertion process by an unskilled patient.

(B) The fabricated MNA being used for dermal interstitial fluid extraction in a human subject. The extracted fluid was collected in the glass capillary tubes (scale bar: 1 cm) (Miller et al., 2018). Adapted with permission from (Miller et al., 2018). Copyright 2018, Springer Nature.

these holders to form the MNAs. Because the MNs are susceptible to fracture during the insertion process, owing to their microscale thickness, the first benefit of using MN holders is protecting the MN, and thus, decreasing the chance of cracking MN during the injection by untrained patients, eliminating the need for the direct supervision of medical clinicians for insertion. Also, the holder applies pressure on the surroundings of the insertion site, enhancing the extraction rate in some cases. The concave geometry showed the best efficiency among the designed profiles with an extraction rate of 0.85 ± 0.64 μL min^{-1} when it was inserted as deep as 1.5 mm. Also, the length of the needles showed no major differences in the amount of extraction (Taylor et al., 2020). In another similar study, ultra-fine needles, lubricated with a silicone lubricant to lessen the pain while insertion, were attached to photopolymer jetting 3D-printed holder arrays to shape the MNAs (Miller et al., 2018). The fabricated MNs were used to extract dermal interstitial fluid from humans and rats. Fluid amounts of up to 20 μL and 60 μL were extracted from human subjects and rats, respectively (Figure 10). The MN with a length of 1.5 mm had the best extraction success percentage, with 31%, compared with 1 mm and 2 mm MNs, with 14% and 16%, respectively.

Signal acquisition

MNs have applications in bio-signal detection such as providing continual point-of-care tests. Early detection of diseases not only can alleviate the number of deaths or disabilities caused by cardiac or metabolic disorders but also reduces healthcare costs for treatments of patients. Electrocardiography (ECG), electromyography (EMG), and electroencephalography (EEG) are vital bio-signals that could be monitored continually. Results acquired from these tests can help cardiovascular, muscular dystrophy, and epilepsy patients, respectively (Ren et al., 2017).

Multiple methods have been proposed for recording bio-signals. Wet electrodes as a conventional method require a time-consuming process of skin preparation and gel usage. Using gel hinders the long-term use of wet electrodes in point-of-care applications. Dry electrodes, on the other hand, as a possible solution for the drawbacks of wet electrodes, suffer from being on rigid substrates, which confine electrodes' flexibility and compatibility with skin. Moreover, large impedance values have been reported for dry flexible electrodes (Wang et al., 2017). The principle of conventional dry electrodes is based on capacitive detection, in which converter amplifiers inherently cause high impedances. This approach requires large equipment as well as auxiliary power sources that make this method a high-cost laboratory method. Understanding the principle of electrode-skin-electrode impedance (ESEI) can solve this limitation. Human skin is encompassed of two distinct layers, the outermost layer, stratum corneum that are dead cells and stratum germinativum (SG) that are active cells. Conventional methods that use wet or dry electrodes on the skin are in touch with the outer layer of skin, SC. Therefore, this type of connection causes background noise and an imprecise signal-to-noise ratio. To surmount this problem, reducing SC thickness by shaving hair and

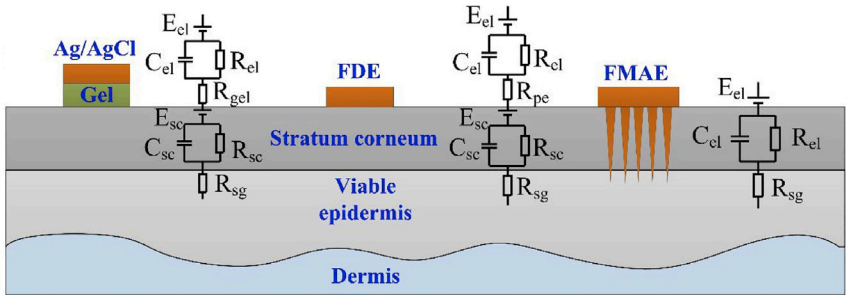

Figure 11. Different layers constituting the skin and circuit model corresponding to different bio-signal recording techniques

Whereas utilizing conventional wet electrodes (e.g., Ag/AgCl probes) require the use of gel, causing allergenic reactions in a number of patients, flexible dry electrode (FDE) probes require skin preparation step (e.g., shaving body hairs), prior to signal acquisition, bringing about unwillingness in patients for the test. However, microneedle arrays (MNA) not only do not need any gel usage or skin preparation, but MNs also do not suffer from background noise and high signal-to-noise rate owing to penetrating layers beneath the outermost layer of skin (Ren et al., 2017). Adapted with permission from (Ren et al., 2017). Copyright 2017, Elsevier.

removing the outmost layer of skin is suggested. These solutions will cause inconvenience for patients. Another possible solution is employing electrolytic gels to penetrate into the SC layer and reach SG to reduce the impedance. However, these gels may cause allergenic reactions and inconvenience to patients in long-term use. Using MNs, on the other hand, eliminates these predicaments (Yu et al., 2009). Because the thickness of the SC layer is 50–100 μm (Wang et al., 2017) and most of the contemporary MNs are longer than the thickness of SC, MNs can penetrate deep into the SG layer to measure signals directly, with minimum impedance. In addition, because MNs penetrate the SC layer, in which there are no blood vessels and nerve endings, patients feel no pain during the insertion process (Hegde et al., 2011). Figure 11 depicts the signal measurement process and the electrical circuit simulation of conventional and MN-based methods (Ren et al., 2017; Yu et al., 2009).

The performance of these methods was compared under stable conditions. A flexible MNA electrode was fabricated to have 36 needles (36-FMAE) by MRDL method, on a flexible substrate as a wearable sensor. To ensure the conductivity and biocompatibility of MNAs, a Ti/Au film was coated on them. Three healthy volunteers recorded their bio-signals by 36-FMAE, flexible dry electrode (FDE), and wet electrode methods, under the same condition. The investigation consisted of four discrete tests (Ren et al., 2017). First, electrode skin interface impedance (EII) was measured with a two-electrode impedance analyzer. Increasing the number of MNs on the array considerably decreased the impedance. This could be attributed to the reduction of multi-parallel impedance as a result of more MNs. Overall, 36-FMAE had the best and lowest impedance compared with that of FDE and wet-electrodes. The second test was an ECG test. Increasing the number of MNs on the array could increase the amplitude of the signal, which is favorable. This effect could be due to the increase in the contact area of needles with the skin because of more MNs. In addition, different types of waves constituting the ECG signal were distinguishable in 36-FMAE because MNs pierce into the skin. Thus, recorded signals by 36-FMAE do not suffer from noise and artifacts caused by moving skin. However, these artifacts are present in FDE and wet electrode signals, which can adversely affect the accuracy of recorded signals. The third test was an EMG measurement, which was performed by using three electrodes on the biceps brachia and elbow. 36-FMAE had the largest signal amplitude. In the case of muscle activation, 36-FMAE traced signals with high fidelity. Finally, the unipolar connection method was used to record EEG signals during an eye-blinking test by an electrode on the earlobe. The shape of the recorded signal by 36-FMAE was analogous to that of the FDE and wet-electrode method. Similar to the other tests, the amplitude of the 36-FMAE signal was larger. Overall, 36-FMAE had an acceptable performance for bio-signal recording when compared with conventional methods. 36-FMAE not only could reduce the motion artifacts and impedance by penetrating the skin but was also cost-effective (Ren et al., 2017).

In another study, a two-step process, direct-metal-laser-sintering (DMLS) 3D printing and polishing, was used to print MNs from medical-grade stainless steel, with 657 μm height and 250 μm base diameter. MNs post-processed with electropolishing after fabrication led to enhancing surface roughness as well

as reducing tip radius from 51 μm to 19 μm. The results of this study corroborated the superiority of MN-based electrodes over conventional wet/dry electrodes for EMG signal acquisition. Furthermore, the advantageous effect of increasing the number of MNs, in an array, on reducing the electrode-skin impedance was emphasized (Krieger et al., 2020).

FUTURE VIEW AND CONCLUSION

Advantages of MNs have recently surged the number of scientific reports regarding diverse types of MNs, including hollow, solid, coated, and dissolvable, with a range of feature sizes for a variety of biomedical applications such as drug delivery, biosignal acquisition, and sample extraction. Moreover, a wide range of MN fabrication methods was proposed: subtractive and additive approaches. This review provides an overview of the working principles of 3D printing methods, highest attainable resolution, supported materials, and advantages as a guideline for the selection of proper fabrication method for future MN applications. Furthermore, the present review provides an overview of the benefits offered by the integration of 3D printing with MNs, applicable 3D printing techniques for MN fabrication, potential applications of MNs, and recent advances.

Regular and contentious monitoring of health and large-scale vaccination are required to control and curb the impact of life-threatening diseases on healthcare systems worldwide. Conventional methods can partially fulfill the demand for regular tests; however, they are associated with low patient compliance, high-cost, and limited accessibility. Substituting present methods with mass-producible, accurate, cost-efficient, point-of-need technologies will substantially reduce healthcare costs and increase life quality globally. MNs are devices with versatile shapes and types that offer numerous benefits such as being low-cost, portable, efficient, precise, and readily available for applications in drug delivery, liquid sample extraction from the body, biosignal acquisition, and point-of-care diagnostics. However, there are some challenges remaining in this area. For example, there is a need for new research on materials that are used to fabricate MNs to increase their ability in the absorption of liquids, for enabling more drug load either in drug delivery applications or in sample extraction (Zhu et al., 2020b). Moreover, the majority of the reported cases have been studied within mimicking tissues and animals.

Despite the fact that current MN fabrication techniques could yield an acceptable resolution, cost-effectiveness, requiring manual steps, demanding high proficiency in the micromanufacturing for proper implementation, and being labor-intensive are existing limitations of conventional methods. 3D printing is a promising approach for MN fabrication because proposed MNs with desired size features can be designed, modified, and fabricated directly, truncating the design and prototyping process by eliminating the need for third-party manufacturing companies. However, slow printing, resolution confinements, limited material choice, and biocompatibility are serious challenges of 3D printing (Chen et al., 2019b; Ligon et al., 2017). Although the terms "3D printing" and "rapid-prototyping" have been used interchangeably, the actual 3D printing process is not as fast as conventional industrial approaches, such as inject molding (Ligon et al., 2017). Moreover, regardless of the substantial attention received by 3D printing, achieving higher resolution is an existing challenge. SLA, TPP, and DLW can produce MNs with acceptable resolutions (5 μm); nevertheless, limited biocompatible materials are supported with these methods, whereas mechanical properties are not of a satisfactory degree (Chia and Wu, 2015; Ligon et al., 2017; Ngo et al., 2018; Yao et al., 2020). Therefore, future studies can be focused on developing faster 3D printing methods without compromising the resolution. By enhancing features of the laser beam, in laser-based methods, and nuzzle features, in extrusion-based methods, the ultimate resolution of printed MNs can be realized.

RESOURCES AVAILABILITY

Lead contact

Further information and requests for resources should be directed to and will be fulfilled by the Lead Contact, Savas Tasoglu (stasoglu@ku.edu.tr).

Materials availability

Not applicable as this is a review article.

Data and code availability

Not applicable as this is a review article.

ACKNOWLEDGMENTS

ST acknowledges Tubitak 2232 International Fellowship for Outstanding Researchers Award (118C391), Alexander von Humboldt Research Fellowship for Experienced Researchers, Marie Skłodowska-Curie Individual Fellowship (101003361), and Royal Academy Newton-Katip Çelebi Transforming Systems Through Partnership award (120N019) for financial support of this research. Opinions, interpretations, conclusions, and recommendations are those of the author and are not necessarily endorsed by the TÜBİTAK. The authors have no other relevant affiliations or financial involvement with any organization or entity with a financial interest in or financial conflict with the subject matter or materials discussed in the manuscript apart from those disclosed.

AUTHOR CONTRIBUTIONS

Writing–Original Draft, S.R.D., M.R.S., and R.R.; Writing–Review & Editing, S.T., A.K.Y., and E.S.; Supervision, S.T. All authors revised and approved the final version of the manuscript.

REFERENCES

Aimar, A., Palermo, A., and Innocenti, B. (2019). The role of 3D printing in medical applications: a state of the art. J. Healthc. Eng. *2019*, 5340616.

Aksit, A., Arteaga, D.N., Arriaga, M., Wang, X., Watanabe, H., Kasza, K.E., Lalwani, A.K., and Kysar, J.W. (2018). In-vitro perforation of the round window membrane via direct 3-D printed microneedles. Biomed. Microdevices *20*, 47.

Ali, R., Mehta, P., Arshad, M., Kucuk, I., Chang, M., and Ahmad, Z. (2020). Transdermal microneedles—a materials perspective. AAPS PharmSciTech *21*, 12.

Amin, R., Knowlton, S., Hart, A., Yenilmez, B., Ghaderinezhad, F., Katebifar, S., Messina, M., Khademhosseini, A., and Tasoglu, S. (2016a). 3D-printed microfluidic devices. Biofabrication *8*, 022001.

Amin, R., Knowlton, S., Yenilmez, B., Hart, A., Joshi, A., and Tasoglu, S. (2016b). Smart-phone attachable, flow-assisted magnetic focusing device. RSC Adv. *6*, 93922–93931.

Baek, S.-H., Shin, J.-H., and Kim, Y.-C. (2017). Drug-coated microneedles for rapid and painless local anesthesia. Biomed. Microdevices *19*, 2.

Bakhshinejad, A. and D'souza, R.M. (2015). A brief comparison between available bio-printing methods. Paper presented at: 2015 IEEE Great Lakes biomedical conference (GLBC) (IEEE).

Balmert, S.C., Carey, C.D., Falo, G.D., Sethi, S.K., Erdos, G., Korkmaz, E., and Falo, L.D. (2020). Dissolving undercut microneedle arrays for multicomponent cutaneous vaccination. J. Controll. Release *317*, 336–346.

Bevers, T.B. (2001). Breast cancer chemoprevention: current clinical practice and future direction. Biomed. Pharmacother. *55*, 559–564.

Bhatnagar, S., Dave, K., and Venuganti, V.V.K. (2017). Microneedles in the clinic. J. Controll. Release *260*, 164–182.

Bhatnagar, S., Gadeela, P.R., Thathireddy, P., and Venuganti, V.V.K. (2019). Microneedle-based drug delivery: materials of construction. J. Chem. Sci. *131*, 90.

Camović, M., Biščević, A., Brčić, I., Borčak, K., Bušatlić, S., Čenanović, N., Dedović, A., Mulalić, A., Osmanlić, M., and Sirbubalo, M. (2019). Coated 3d printed PLA microneedles as transdermal drug delivery systems. Paper presented at: International Conference on Medical and Biological Engineering (Springer).

Caudill, C.L., Perry, J.L., Tian, S., Luft, J.C., and DeSimone, J.M. (2018). Spatially controlled coating of continuous liquid interface production microneedles for transdermal protein delivery. J. Controll. Release *284*, 122–132.

Chambers, R. (1921). Microdissection studies, III. Some problems in the maturation and fertilization of the echinoderm egg. Biol. Bull. *41*, 318–350.

Chang, H., Zheng, M., Yu, X., Than, A., Seeni, R.Z., Kang, R., Tian, J., Khanh, D.P., Liu, L., Chen, P., et al. (2017). A swellable microneedle patch to rapidly extract skin interstitial fluid for timely metabolic analysis. Adv. Mater. *29*, 1702243.

Chen, H., Wu, B., Zhang, M., Yang, P., Yang, B., Qin, W., Wang, Q., Wen, X., Chen, M., Quan, G., et al. (2019a). A novel scalable fabrication process for the production of dissolving microneedle arrays. Drug Deliv. Transl. Res. *9*, 240–248.

Chen, J., Liu, C.-Y., Wang, X., Sweet, E., Liu, N., Gong, X., and Lin, L. (2020). 3D printed microfluidic devices for circulating tumor cells (CTCs) isolation. Biosens. Bioelectron. *150*, 111900.

Chen, Z., Li, Z., Li, J., Liu, C., Lao, C., Fu, Y., Liu, C., Li, Y., Wang, P., and He, Y. (2019b). 3D printing of ceramics: a review. J. Eur. Ceram. Soc. *39*, 661–687.

Chen, Z., Ren, L., Li, J., Yao, L., Chen, Y., Liu, B., and Jiang, L. (2018). Rapid fabrication of microneedles using magnetorheological drawing lithography. Acta Biomater. *65*, 283–291.

Chen, Z., Ye, R., Yang, J., Lin, Y., Lee, W., Li, J., Ren, L., Liu, B., and Jiang, L. (2019c). Rapidly fabricated microneedle arrays using magnetorheological drawing lithography for transdermal drug delivery. ACS Biomater. Sci. Eng. *5*, 5506–5513.

Chia, H.N., and Wu, B.M. (2015). Recent advances in 3D printing of biomaterials. J. Biol. Eng. *9*, 4.

Chiang, H., Yu, M., Aksit, A., Wang, W., Stern-Shavit, S., Kysar, J.W., and Lalwani, A.K. (2020). 3D-printed microneedles create precise perforations in human round window membrane in situ. Otol. Neurotol. *41*, 277–284.

Cordeiro, A.S., Tekko, I.A., Jomaa, M.H., Vora, L., McAlister, E., Volpe-Zanutto, F., Nethery, M., Baine, P.T., Mitchell, N., and McNeill, D.W. (2020). Two-photon polymerisation 3D printing of microneedle array templates with versatile designs: application in the development of polymeric drug delivery systems. Pharm. Res. *37*, 1–15.

Dhinakaran, V., Kumar, K.M., Ram, P.B., Ravichandran, M., and Vinayagamoorthy, M. (2020). A review on recent advancements in fused deposition modeling. Mater. Today Proc. *27*, 752–756.

Donnelly, R.F., Majithiya, R., Singh, T.R.R., Morrow, D.I.J., Garland, M.J., Demir, Y.K., Migalska, K., Ryan, E., Gillen, D., Scott, C.J., et al. (2011). Design, optimization and characterisation of polymeric microneedle arrays prepared by a novel laser-based micromoulding technique. Pharm. Res. *28*, 41–57.

Douroumis, D. (2019). 3D Printing of Pharmaceutical and Medical Applications: A New Era (Springer).

Economidou, S.N., Pere, C.P.P., Reid, A., Uddin, M.J., Windmill, J.F.C., Lamprou, D.A., and Douroumis, D. (2019). 3D printed microneedle patches using stereolithography (SLA) for intradermal insulin delivery. Mater. Sci. Eng. C Mater. Biol. Appl. *102*, 743–755.

Farhan, S.A., Shaikh, A.T., Zia, M., Kahara, B.R., Muneer, R., Rehman, M., Mubashir, A., Sadiq, H., Siddiqui, D.-E.A., Haseeb, S.M., et al. (2017). Prevalence and predictors of home use of glucometers in diabetic patients. Cureus *9*, e1330.

Fernandes, D. (2005). Minimally invasive percutaneous collagen induction. Oral Maxillofac. Surg. Clin. *17*, 51–63.

Gallo, R.L. (2017). Human skin is the largest epithelial surface for interaction with microbes. J. Invest. Dermatol. *137*, 1213–1214.

García-López, E., Siller, H.R., and Rodríguez, C.A. (2018). Study of the fabrication of AISI 316L microneedle arrays. Procedia Manuf. *26*, 117–124.

Geng, Q., Wang, D., Chen, P., and Chen, S.-C. (2019). Ultrafast multi-focus 3-D nano-fabrication based on two-photon polymerization. Nat. Commun. *10*, 1–7.

Gerstel, M.S., and Place, V.A. (1976). Drug Delivery Device (Google Patents).

Ghaderinezhad, F., Koydemir, H.C., Tseng, D., Karinca, D., Liang, K., Ozcan, A., and Tasoglu, S. (2020). Sensing of electrolytes in urine using a miniaturized paper-based device. Sci. Rep. *10*, 1–9.

Gholami, S., Mohebi, M.-M., Hajizadeh-Saffar, E., Ghanian, M.-H., Zarkesh, I., and Baharvand, H. (2019). Fabrication of microporous inorganic microneedles by centrifugal casting method for transdermal extraction and delivery. Int. J. Pharm. *558*, 299–310.

Gissibl, T., Thiele, S., Herkommer, A., and Giessen, H. (2016). Two-photon direct laser writing of ultracompact multi-lens objectives. Nat. Photon. *10*, 554–560.

Gong, J., Schuurmans, C.C., van Genderen, A.M., Cao, X., Li, W., Cheng, F., He, J.J., López, A., Huerta, V., and Manríquez, J. (2020). Complexation-induced resolution enhancement of 3D-printed hydrogel constructs. Nat. Commun. *11*, 1–14.

Han, D., Morde, R.S., Mariani, S., La Mattina, A.A., Vignali, E., Yang, C., Barillaro, G., and Lee, H. (2020). 4D printing of a bioinspired microneedle array with backward-facing barbs for enhanced tissue adhesion. Adv. Funct. Mater. *30*, 1909197.

Hegde, N.R., Kaveri, S.V., and Bayry, J. (2011). Recent advances in the administration of vaccines for infectious diseases: microneedles as painless delivery devices for mass vaccination. Drug Discov. Today *16*, 1061–1068.

Henry, S., McAllister, D.V., Allen, M.G., and Prausnitz, M.R. (1998). Microfabricated microneedles: a novel approach to transdermal drug delivery. J. Pharm. Sci. *87*, 922–925.

Indermun, S., Luttge, R., Choonara, Y.E., Kumar, P., Du Toit, L.C., Modi, G., and Pillay, V. (2014). Current advances in the fabrication of microneedles for transdermal delivery. J. Controll. Release *185*, 130–138.

Jacinto, T.A., Rodrigues, C.F., Moreira, A.F., Miguel, S.P., Costa, E.C., Ferreira, P., and Correia, I.J. (2020). Hyaluronic acid and Vitamin E polyethylene glycol succinate functionalized gold-core silica shell nanorods for cancer targeted photothermal therapy. Colloids Surf B Biointerfaces *188*, 110778.

Jain, A., Mathur, T., Pandian, N.K., and Selahi, A. (2020). Organ-on-a-chip and 3D printing as preclinical models for medical research and practice. In Precision Medicine for Investigators, Practitioners and Providers (Elsevier), pp. 83–95.

Javaid, M., and Haleem, A. (2020). 3D printing applications towards the required challenge of stem cells printing. Clin. Epidemiol. Glob. Health *8*, 862–867.

Johnson, A.R., Caudill, C.L., Tumbleston, J.R., Bloomquist, C.J., Moga, K.A., Ermoshkin, A., Shirvanyants, D., Mecham, S.J., Luft, J.C., and DeSimone, J.M. (2016). Single-step fabrication of computationally designed microneedles by continuous liquid interface production. PLoS One *11*, e0162518.

Johnson, A.R., and Procopio, A.T. (2019). Low cost additive manufacturing of microneedle masters. 3D Print. Med. *5*, 2.

Joseph, J., Deshmukh, K., Tung, T., Chidambaram, K., and Pasha, S.K. (2019). 3D printing technology of polymer composites and hydrogels for artificial skin tissue implementations. In Polymer Nanocomposites in Biomedical Engineering, K. Sadasivuni, D. Ponnamma, M. Rajan, B. Ahmed, and M. Al-Maadeed, eds. (Springer), pp. 205–233.

Kabashima, K., Honda, T., Ginhoux, F., and Egawa, G. (2019). The immunological anatomy of the skin. Nat. Rev. Immunol. *19*, 19–30.

Kanakasabapathy, M.K., Thirumalaraju, P., Bormann, C.L., Kandula, H., Dimitriadis, I., Souter, I., Yogesh, V., Pavan, S.K.S., Yarravarapu, D., Gupta, R., et al. (2019). Development and evaluation of inexpensive automated deep learning-based imaging systems for embryology. Lab. Chip *19*, 4139–4145.

Kathuria, H., Kang, K., Cai, J., and Kang, L. (2020). Rapid microneedle fabrication by heating and photolithography. Int. J. Pharm. *575*, 118992.

Kavaldzhiev, M., Perez, J.E., Ivanov, Y., Bertoncini, A., Liberale, C., and Kosel, J. (2017). Biocompatible 3D printed magnetic micro needles. Biomed. Phys. Eng. Express *3*, 025005.

Kim, H., Seong, K.-Y., Lee, J.H., Park, W., Yang, S.Y., and Hahn, S.K. (2019). Biodegradable microneedle patch delivering antigenic peptide–hyaluronate conjugate for cancer immunotherapy. ACS Biomater. Sci. Eng. *5*, 5150–5158.

Kim, Y.-C., Park, J.-H., and Prausnitz, M.R. (2012). Microneedles for drug and vaccine delivery. Adv. Drug Deliv. Rev. *64*, 1547–1568.

Knowlton, S., Anand, S., Shah, T., and Tasoglu, S. (2018). Bioprinting for neural tissue engineering. Trends Neurosci. *41*, 31–46.

Knowlton, S., Joshi, A., Syrrist, P., Coskun, A.F., and Tasoglu, S. (2017a). 3D-printed smartphone-based point of care tool for fluorescence-and magnetophoresis-based cytometry. Lab. Chip *17*, 2839–2851.

Knowlton, S., Joshi, A., Yenilmez, B., Ozbolat, I.T., Chua, C.K., Khademhosseini, A., and Tasoglu, S. (2016a). Advancing cancer research using bioprinting for tumor-on-a-chip platforms. Int. J. Bioprint. *2* (2), 3–8.

Knowlton, S., Onal, S., Yu, C.H., Zhao, J.J., and Tasoglu, S. (2015a). Bioprinting for cancer research. Trends Biotechnol. *33*, 504–513.

Knowlton, S., Sencan, I., Aytar, Y., Khoory, J., Heeney, M., Ghiran, I., and Tasoglu, S. (2015b). Sickle cell detection using a smartphone. Sci. Rep. *5*, 15022.

Knowlton, S., and Tasoglu, S. (2016). A bioprinted liver-on-a-chip for drug screening applications. Trends Biotechnol. *34*, 681–682.

Knowlton, S., Yenilmez, B., Anand, S., and Tasoglu, S. (2017b). Photocrosslinking-based bioprinting: examining crosslinking schemes. Bioprinting *5*, 10–18.

Knowlton, S., Yenilmez, B., and Tasoglu, S. (2016b). Towards single-step biofabrication of organs on a chip via 3D printing. Trends Biotechnol. *34*, 685–688.

Knowlton, S., Yu, C.H., Ersoy, F., Emadi, S., Khademhosseini, A., and Tasoglu, S. (2016c). 3D-printed microfluidic chips with patterned, cell-laden hydrogel constructs. Biofabrication *8*, 025019.

Knowlton, S., Yu, C.H., Jain, N., Ghiran, I.C., and Tasoglu, S. (2015c). Smart-phone based magnetic levitation for measuring densities. PLoS One *10*, e0134400.

Knowlton, S.M., Sadasivam, M., and Tasoglu, S. (2015d). Microfluidics for sperm research. Trends Biotechnol. *33*, 221–229.

Krieger, K.J., Bertollo, N., Dangol, M., Sheridan, J.T., Lowery, M.M., and O'Cearbhaill, E.D. (2019). Simple and customizable method for fabrication of high-aspect ratio microneedle molds using low-cost 3D printing. Microsyst. Nanoeng. *5*, 42.

Krieger, K.J., Liegey, J., Cahill, E.M., Bertollo, N., Lowery, M.M., and O'Cearbhaill, E.D. (2020). Development and evaluation of 3D-printed dry microneedle electrodes for surface electromyography. Adv. Mater. Technol. *5*, 2000518.

Lambert, P.H., and Laurent, P.E. (2008). Intradermal vaccine delivery: will new delivery systems transform vaccine administration? Vaccine *26*, 3197–3208.

Lee, K.-S., Kim, R.H., Prabhakaran, P., Yang, D.-Y., Lim, T.W., and Park, S.H. (2007). Two-photon stereolithography. J. Nonlinear Opt. Phys. Mater. *16*, 59–73.

Lepowsky, E., and Tasoglu, S. (2018). 3D printing for drug manufacturing: a perspective on the future of pharmaceuticals. Int. J. Bioprint. *4*, 119.

Li, C.G., Lee, C.Y., Lee, K., and Jung, H. (2013). An optimized hollow microneedle for minimally invasive blood extraction. Biomed. Microdevices *15*, 17–25.

Li, J., Liu, B., Zhou, Y., Chen, Z., Jiang, L., Yuan, W., and Liang, L. (2017). Fabrication of a Ti porous microneedle array by metal injection molding for transdermal drug delivery. PLoS One *12*, e0172043.

Li, Y., Zhang, H., Yang, R., Laffitte, Y., Schmill, U., Hu, W., Kaddoura, M., Blondeel, E.J.M., and Cui, B. (2019). Fabrication of sharp silicon hollow microneedles by deep-reactive ion etching towards minimally invasive diagnostics. Microsyst. Nanoeng. *5*, 41.

Lightman, S., Hurvitz, G., Gvishi, R., and Arie, A. (2017). Miniature wide-spectrum mode sorter for vortex beams produced by 3D laser printing. Optica *4*, 605–610.

Ligon, S.C., Liska, R., Stampfl, J.r., Gurr, M., and Mulhaupt, R. (2017). Polymers for 3D printing and customized additive manufacturing. Chem. Rev. *117*, 10212–10290.

Lim, J., Tahk, D., Yu, J., Min, D.-H., and Jeon, N.L. (2018). Design rules for a tunable merged-tip microneedle. Microsyst. Nanoeng. *4*, 1–10.

Lim, S.H., Ng, J.Y., and Kang, L. (2017). Three-dimensional printing of a microneedle array on personalized curved surfaces for dual-pronged treatment of trigger finger. Biofabrication *9*, 015010.

Lin, Y.-H., Lee, I.-C., Hsu, W.-C., Hsu, C.-H., Chang, K.-P., and Gao, S.-S. (2016). Rapid fabrication method of a microneedle mold with controllable needle height and width. Biomed. Microdevices *18*, 85.

Liu, W., Zhong, Z., Hu, N., Zhou, Y., Maggio, L., Miri, A.K., Fragasso, A., Jin, X., Khademhosseini, A., and Zhang, Y.S. (2018). Coaxial extrusion bioprinting of 3D microfibrous constructs with cell-favorable gelatin methacryloyl microenvironments. Biofabrication *10*, 024102.

Lu, Y., Mantha, S.N., Crowder, D.C., Chinchilla, S., Shah, K.N., Yun, Y.H., Wicker, R.B., and Choi, J.-W. (2015). Microstereolithography and characterization of poly (propylene fumarate)-based drug-loaded microneedle arrays. Biofabrication *7*, 045001.

Luzuriaga, M.A., Berry, D.R., Reagan, J.C., Smaldone, R.A., and Gassensmith, J.J. (2018). Biodegradable 3D printed polymer microneedles for transdermal drug delivery. Lab. Chip *18*, 1223–1230.

Mansor, N.H.A., Markom, M.A., Tan, E.S.M.M., and Adom, A.H. (2019). Design and Fabrication of Biodegradable Microneedle Using 3D Rapid Prototyping Printer. Paper presented at: Journal of Physics: Conference Series (IOP Publishing).

Mazzoli, A. (2013). Selective laser sintering in biomedical engineering. Med. Biol. Eng. Comput. *51*, 245–256.

McAllister, D.V., Wang, P.M., Davis, S.P., Park, J.-H., Canatella, P.J., Allen, M.G., and Prausnitz, M.R. (2003). Microfabricated needles for transdermal delivery of macromolecules and nanoparticles: fabrication methods and transport studies. Proc. Natl. Acad. Sci. U S A *100*, 13755–13760.

Mikszta, J.A., Alarcon, J.B., Brittingham, J.M., Sutter, D.E., Pettis, R.J., and Harvey, N.G. (2002). Improved genetic immunization via micromechanical disruption of skin-barrier function and targeted epidermal delivery. Nat. Med. *8*, 415–419.

Miller, P.R., Taylor, R.M., Tran, B.Q., Boyd, G., Glaros, T., Chavez, V.H., Krishnakumar, R., Sinha, A., Poorey, K., Williams, K.P., et al. (2018). Extraction and biomolecular analysis of dermal interstitial fluid collected with hollow microneedles. Commun. Biol. *1*, 173.

Miyano, T., Tobinaga, Y., Kanno, T., Matsuzaki, Y., Takeda, H., Wakui, M., and Hanada, K. (2005). Sugar micro needles as transdermic drug delivery system. Biomed. Microdevices *7*, 185–188.

Mojeiko, G., de Brito, M., Salata, G.C., and Lopes, L.B. (2019). Combination of microneedles and microemulsions to increase celecoxib topical delivery for potential application in chemoprevention of breast cancer. Int. J. Pharm. *560*, 365–376.

Morde, R.S. (2018). Micro-3D Printing of Bio-Inspired Microneedle with Enhanced Adhesion Capabilities (Rutgers University-School of Graduate Studies).

Moussi, K., Bukhamsin, A., Hidalgo, T., and Kosel, J. (2020). Biocompatible 3D printed microneedles for transdermal, intradermal, and percutaneous applications. Adv. Eng. Mater. *22*, 1901358.

Mukerjee, E., Collins, S., Isseroff, R.R., and Smith, R. (2004). Microneedle array for transdermal biological fluid extraction and in situ analysis. Sens. Actuator. A Phys. *114*, 267–275.

Nejad, H.R., Sadeqi, A., Kiaee, G., and Sonkusale, S. (2018). Low-cost and cleanroom-free fabrication of microneedles. Microsyst. Nanoeng. *4*, 1–7.

Ngo, T.D., Kashani, A., Imbalzano, G., Nguyen, K.T.Q., and Hui, D. (2018). Additive manufacturing (3D printing): a review of materials, methods, applications and challenges. Composite. B Eng. *143*, 172–196.

Ni, G., Ge, X., Liu, L., Zhang, J., Wang, X., Liu, J., Liu, L., and Liu, Y. (2020). Towards indicating human skin state in vivo using geometry-dependent spectroscopic contrast imaging. IEEE Photon. Technol. Lett. *32*, 697–700.

Nicholas, D., Logan, K.A., Sheng, Y., Gao, J., Farrell, S., Dixon, D., Callan, B., McHale, A.P., and Callan, J.F. (2018). Rapid paper based colorimetric detection of glucose using a hollow microneedle device. Int. J. Pharm. *547*, 244–249.

Norman, J.J., Arya, J.M., McClain, M.A., Frew, P.M., Meltzer, M.I., and Prausnitz, M.R. (2014). Microneedle patches: usability and acceptability for self-vaccination against influenza. Vaccine *32*, 1856–1862.

Ochoa, M., Zhou, J., Rahimi, R., Badwaik, V., Thompson, D., and Ziaie, B. (2015). Rapid 3D-print-and-shrink fabrication of biodegradable microneedles with complex geometries. Paper presented at: 2015 Transducers - 2015 18th International Conference on Solid-State Sensors, Actuators and Microsystems (TRANSDUCERS).

Olatunji, O., Das, D.B., Garland, M.J., Belaid, L., and Donnelly, R.F. (2013). Influence of array interspacing on the force required for successful microneedle skin penetration: theoretical and practical approaches. J. Pharm. Sci. *102*, 1209–1221.

Park, C., Kim, M.H., Hong, S.M., Go, J.S., and Shin, B.S. (2015). A study on the comparison mechanical properties of 3D printing prototypes with laminating direction. J. Korean Soc. Manuf. Technol. Eng. *24*, 334–341.

Pere, C.P.P., Economidou, S.N., Lall, G., Ziraud, C., Boateng, J.S., Alexander, B.D., Lamprou, D.A., and Douroumis, D. (2018). 3D printed microneedles for insulin skin delivery. Int. J. Pharm. *544*, 425–432.

Pistor, M.L.P. (1975). Device for Cutaneous Therapeutic Treatment (Google Patents).

Potluri, V., Kathiresan, P.S., Kandula, H., Thirumalaraju, P., Kanakasabapathy, M.K., Pavan, S.K.S., Yarravarapu, D., Soundararajan, A., Baskar, K., Gupta, R., et al. (2018). An inexpensive smartphone-based device for point-of-care ovulation testing. Lab. Chip *19*, 59–67.

Prausnitz, M.R. (2004). Microneedles for transdermal drug delivery. Adv. Drug Deliv. Rev. *56*, 581–587.

Prausnitz, M.R., and Langer, R. (2008). Transdermal drug delivery. Nat. Biotechnol. *26*, 1261–1268.

Quan, H., Zhang, T., Xu, H., Luo, S., Nie, J., and Zhu, X. (2020). Photo-curing 3D printing technique and its challenges. Bioactive Mater. *5*, 110–115.

Queiroz, M.L.B., Shanmugam, S., Santos, L.N.S., Campos, C.d.A., Santos, A.M., Batista, M.S., Araújo, A.A.d.S., and Serafini, M.R. (2020). Microneedles as an alternative technology for transdermal drug delivery systems: a patent review. Expert Opin. Ther. Pat. *30*, 433–452.

Rad, Z.F., Nordon, R.E., Anthony, C.J., Bilston, L., Prewett, P.D., Arns, J.-Y., Arns, C.H., Zhang, L., and Davies, G.J. (2017). High-fidelity replication of thermoplastic microneedles with open microfluidic channels. Microsyst. Nanoeng. *3*, 1–11.

Ren, L., Jiang, Q., Chen, Z., Chen, K., Xu, S., Gao, J., and Jiang, L. (2017). Flexible microneedle array electrode using magnetorheological drawing lithography for bio-signal monitoring. Sens. Actuator. A Phys. *268*, 38–45.

Russell, L.M., Wiedersberg, S., and Delgado-Charro, M.B. (2008). The determination of stratum corneum thickness: an alternative approach. Eur. J. Pharm. Biopharm. *69*, 861–870.

Sears, N.A., Seshadri, D.R., Dhavalikar, P.S., and Cosgriff-Hernandez, E. (2016). A review of three-dimensional printing in tissue engineering. Tissue Eng. B Rev. *22*, 298–310.

Semin, J.N., Palm, D., Smith, L.M., and Ruttle, S. (2020). Understanding breast cancer survivors' financial burden and distress after financial assistance. Support Care Cancer *28*, 1–8.

Serex, L., Bertsch, A., and Renaud, P. (2018). Microfluidics: a new layer of control for extrusion-based 3D printing. Micromachines *9*, 86.

Tabriz, A.G., Douroumis, D., and Boateng, J. (2020). 3D printed scaffolds for wound healing and tissue regeneration. In Therapeutic Dressings and Wound Healing Applications, J. Boateng, ed. (Wiley), pp. 385–398.

Takeuchi, K., Takama, N., Kim, B., Sharma, K., Paul, O., and Ruther, P. (2019). Microfluidic chip to interface porous microneedles for ISF collection. Biomed. Microdevices *21*, 28.

Tasoglu, S., and Demirci, U. (2013). Bioprinting for stem cell research. Trends Biotechnol. *31*, 10–19.

Taylor, R.M., Maharjan, D., Moreu, F., and Baca, J.T. (2020). Parametric study of 3D printed

microneedle (MN) holders for interstitial fluid (ISF) extraction. Microsyst. Technol. *26*, 2067–2073.

Tejavibulya, N., Colburn, D.A., Marcogliese, F.A., Yang, K.-A., Guo, V., Chowdhury, S., Stojanovic, M.N., and Sia, S.K. (2019). Hydrogel microfilaments toward intradermal health monitoring. Iscience *21*, 328–340.

Tran, K.T., Gavitt, T.D., Farrell, N.J., Curry, E.J., Mara, A.B., Patel, A., Brown, L., Kilpatrick, S., Piotrowska, R., and Mishra, N. (2020). Transdermal microneedles for the programmable burst release of multiple vaccine payloads. Nat. Biomed. Eng. 1–10. https://doi.org/10.1038/s41551-020-00650-4.

Uddin, M.J., Scoutaris, N., Economidou, S.N., Giraud, C., Chowdhry, B.Z., Donnelly, R.F., and Douroumis, D. (2020). 3D printed microneedles for anticancer therapy of skin tumours. Mater. Sci. Eng. C Mater. Biol. Appl. *107*, 110248.

Vincze, G., Barner, J.C., and Lopez, D. (2004). Factors associated with adherence to self-monitoring of blood glucose among persons with diabetes. Diabetes Educ. *30*, 112–125.

Wang, D., Wang, T., Liu, J., Yu, H., Jiao, S., Feng, B., Zhou, F., Fu, Y., Yin, Q., and Zhang, P. (2016). Acid-activatable versatile micelleplexes for PD-L1 blockade-enhanced cancer photodynamic immunotherapy. Nano Lett. *16*, 5503–5513.

Wang, P.M., Cornwell, M., and Prausnitz, M.R. (2005). Minimally invasive extraction of dermal interstitial fluid for glucose monitoring using microneedles. Diabetes Technol. Ther. *7*, 131–141.

Wang, R., Jiang, X., Wang, W., and Li, Z. (2017). A microneedle electrode array on flexible substrate for long-term EEG monitoring. Sens. Actuator. B Chem. *244*, 750–758.

Wu, M., Zhang, Y., Huang, H., Li, J., Liu, H., Guo, Z., Xue, L., Liu, S., and Lei, Y. (2020). Assisted 3D printing of microneedle patches for minimally invasive glucose control in diabetes. Mater. Sci. Eng. C Mater. Biol. Appl. *117*, 111299.

Xenikakis, I., Tzimtzimis, M., Tsongas, K., Andreadis, D., Demiri, E., Tzetzis, D., and Fatouros, D.G. (2019). Fabrication and finite element analysis of stereolithographic 3D printed microneedles for transdermal delivery of model dyes across human skin in vitro. Eur. J. Pharm. Sci. *137*, 104976.

Yang, J., Liu, X., Fu, Y., and Song, Y. (2019). Recent advances of microneedles for biomedical applications: drug delivery and beyond. Acta Pharm. Sin. B *9*, 469–483.

Yao, W., Li, D., Zhao, Y., Zhan, Z., Jin, G., Liang, H., and Yang, R. (2020). 3D printed multi-functional hydrogel microneedles based on high-precision digital light processing. Micromachines *11*, 17.

Yendeti, B., and Soma, V.R. (2020). Direct fabrication of sub-100 nm nanoneedles in silver using femtosecond laser direct writing. Def. Sci. J. *70*, 197–200.

Yenilmez, B., Knowlton, S., and Tasoglu, S. (2016a). Self-contained handheld magnetic platform for point of care cytometry in biological samples. Adv. Mater. Technol. *1*, 1600144.

Yenilmez, B., Knowlton, S., Yu, C.H., Heeney, M.M., and Tasoglu, S. (2016b). Label-free sickle cell disease diagnosis using a low-cost, handheld platform. Adv. Mater. Technol. *1*, 1600100.

Yeung, C., Chen, S., King, B., Lin, H., King, K., Akhtar, F., Diaz, G., Wang, B., Zhu, J., and Sun, W. (2019). A 3D-printed microfluidic-enabled hollow microneedle architecture for transdermal drug delivery. Biomicrofluidics *13*, 064125.

You, S., Li, J., Zhu, W., Yu, C., Mei, D., and Chen, S. (2018). Nanoscale 3D printing of hydrogels for cellular tissue engineering. J. Mater. Chem. B *6*, 2187–2197.

Yu, L.M., Tay, F.E.H., Guo, D.G., Xu, L., and Yap, K.L. (2009). A microfabricated electrode with hollow microneedles for ECG measurement. Sens. Actuator. A Phys. *151*, 17–22.

Zhang, J., Hu, Q., Wang, S., Tao, J., and Gou, M. (2020). Digital light processing based three-dimensional printing for medical applications. Int. J. Bioprint. *6*, 242.

Zhang, L., Yang, G., Johnson, B.N., and Jia, X. (2019). Three-dimensional (3D) printed scaffold and material selection for bone repair. Acta Biomater. *84*, 16–33.

Zhu, J., Zhou, X., Kim, H.J., Qu, M., Jiang, X., Lee, K., Ren, L., Wu, Q., Wang, C., and Zhu, X. (2020a). Gelatin methacryloyl microneedle patches for minimally invasive extraction of skin interstitial fluid. Small *16*, 1905910.

Zhu, J., Zhou, X., Libanori, A., and Sun, W. (2020b). Microneedle-based bioassays. Nanoscale Adv. *2*, 4295–4304.